

# Mirage: A Multi-Level Superoptimizer for Tensor Programs

Mengdi Wu   Xinhao Cheng   Shengyu Liu<sup>†</sup>   Chunan Shi<sup>†</sup>   Jianan Ji  
 Kit Ao   Praveen Velliengiri<sup>‡</sup>   Xupeng Miao<sup>#</sup>   Oded Padon<sup>◊</sup>   Zhihao Jia

*Carnegie Mellon University*   *Peking University*<sup>†</sup>  
*Pennsylvania State University*<sup>‡</sup>   *Purdue University*<sup>#</sup>   *Weizmann Institute of Science*<sup>◊</sup>

## Abstract

We introduce Mirage, the first multi-level superoptimizer for tensor programs. A key idea in Mirage is  $\mu$ Graphs, a uniform representation of tensor programs at the kernel, thread block, and thread levels of the GPU compute hierarchy.  $\mu$ Graphs enable Mirage to discover novel optimizations that combine algebraic transformations, schedule transformations, and generation of new custom kernels. To navigate the large search space, Mirage introduces a pruning technique based on abstraction that significantly reduces the search space and provides a certain optimality guarantee. To ensure that the optimized  $\mu$ Graph is equivalent to the input program, Mirage introduces a probabilistic equivalence verification procedure with strong theoretical guarantees. Our evaluation shows that Mirage outperforms existing approaches by 1.1-2.9 $\times$  even for DNNs that are widely used and heavily optimized. Mirage is publicly available at <https://github.com/mirage-project/mirage>.

## 1 Introduction

Enabling high-performance execution of deep neural networks (DNNs) on GPUs is critical for modern ML applications. Today’s DNN frameworks generally specify DNN computation using tensor programs, which are directed acyclic graphs whose nodes and edges represent tensor algebra operators (e.g., matrix multiplications) and tensors (i.e.,  $n$ -dimensional array) shared between operators.

To optimize an input tensor program, existing frameworks (e.g., PyTorch [31] and TensorFlow [9]) use manually designed rules to map the tensor program to expert-written GPU kernels. These approaches generally require extensive engineering efforts to design and implement optimization rules, and may miss some optimization opportunities. To address these challenges, recent work introduced *automated* approaches to optimizing tensor programs by searching over a comprehensive space of program transformations and applying them based on their performance on target GPUs. These approaches generally fall into two categories.

The first category of work, including Halide [32], TVM [13], and Ansor [46], is motivated by the idea of algorithm and schedule separation<sup>1</sup> introduced in Halide and optimizes the *schedule* of a tensor program while fixing the algorithm. For a given algorithm, these optimizers automatically generate performant kernels by searching for possible strategies to execute the kernel on the target hardware. However, due to the linear algebra nature of DNNs, a tensor program can be represented by a wide spectrum of mathematically equivalent algorithms, and existing schedule-based optimizers only consider kernels whose algorithms are manually specified by users, resulting in missed optimization opportunities.

The second category of work, including TASO [24], Grappler [3], Tensat [43], and PET [41], considers *algebraic transformations*, which exploit mathematical equivalence between different algorithms for a tensor program. Example algebraic transformations include (1) converting a linear algebra operator into another such as a convolution to a matrix multiplication, (2) fusing multiple operators to reduce memory access and kernel overhead, and (3) reorganizing operators based on commutativity, associativity, and distributivity. These optimizers perform algebraic transformations at the algorithm level and require programmers to manually define the set of available kernels and their implementations. They are thus limited by the performance of the provided kernels.

All existing automated optimization approaches, from both categories, still require programmers to manually specify a set of kernels (each defined by a tensor function), and then explore the search space of algebraic *or* schedule transformations. However, some advanced performance optimizations require coordinated transformations at the kernel, thread block, and thread levels of the GPU compute hierarchy, and involve introducing completely new kernel computations (e.g., a custom kernel that decomposes standard kernels and fuses only some of their computations). Such optimizations are not part of the search space of existing automated methods and must still be implemented manually.

<sup>1</sup>In the schedule optimization literature, an algorithm describes what to compute in a kernel and a schedule specifies how to compute the kernel.

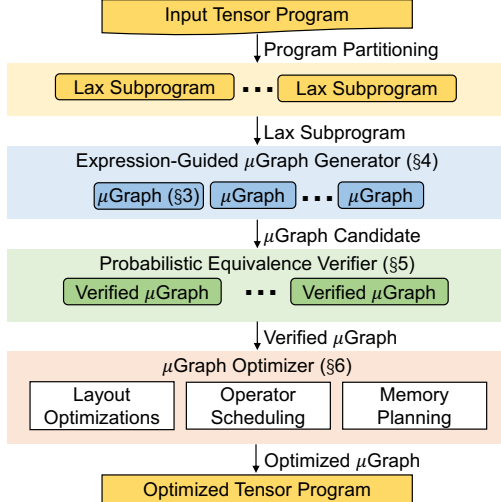


Figure 1: An overview of Mirage.

One such example is FlashAttention [17] (see §8.2 for details), which optimizes attention [42] on GPUs by reordering operators at the algorithm level (algebraic transformations), reorganizing the computation across GPU kernels (yielding new custom kernels), and adapting the parallelization strategy of each kernel to the GPU architecture (schedule transformations). The transformations required for this example cannot be automatically discovered by existing frameworks and must therefore be implemented manually. An implementation of FlashAttention in Triton [39], a widely used tensor program optimizer, includes more than 700 lines of code [8].

We present Mirage, the first *multi-level superoptimizer* for tensor programs. Mirage is able to automatically discover and verify sophisticated optimizations of tensor programs that require joint optimization of algebraic transformations, schedule transformations, and the discovery of new custom kernels.

A key idea in Mirage is *μGraphs*, a *hierarchical graph representation* that specifies a tensor program at multiple levels of the GPU compute hierarchy. By uniformly treating the kernel, thread block, and thread levels, *μGraphs* can capture both algebraic and schedule transformations across these levels. Moreover, optimizing a *μGraph* can introduce new custom kernels, which go beyond both algebraic and schedule transformations. For example, Mirage automatically discovers the *μGraphs* that represent FlashAttention [17] and its inference variant FlashDecoding [5] as well as other *μGraphs* that outperform these manually designed kernels by up to  $3.5 \times$  for certain use cases. Most of these Mirage-discovered optimizations are outside the search space of existing approaches.

Figure 1 shows an overview of Mirage. Mirage first splits an input tensor program into subprograms that fall into the restricted LAX fragment. The LAX fragment, formally defined in §5, includes multi-linear operators such as matrix multiplication and convolution, division (which is useful for

normalizations), and limited use of exponentiation (which is useful for activations). The partitioning into LAX subprograms reduces the optimization search space while preserving most optimization opportunities; it also enables Mirage’s probabilistic equivalence verifier.

**Expression-guided *μGraph* generator.** For each LAX subprogram, Mirage’s *expression-guided generator* uses an exhaustive search to find possible *μGraphs* equivalent to it. A key challenge Mirage has to address is its significantly larger search space compared to prior superoptimization techniques for ML. For example, TASO [24] and PET [41] only search for tensor programs at the kernel level by using a fixed set of pre-defined kernels, while Mirage simultaneously considers superoptimization at the kernel, thread block, and thread levels. To efficiently navigate this significantly larger and more complex search space, Mirage introduces a novel pruning technique based on *abstract expressions*. This approach greatly reduces the number of *μGraphs* Mirage has to consider while providing a theoretical guarantee on the optimality of the discovered *μGraphs* (§4.3).

**Probabilistic equivalence verifier.** For a *μGraph* discovered by Mirage, verifying its functional equivalence with the input program introduces another challenge, since the input and output tensors of a program include up to many millions of elements. A key idea behind Mirage is *probabilistic equivalence verification*, which performs random tests over finite fields to check equivalence between *μGraphs*. While random tests can hardly provide any correctness guarantees for general programs, Mirage relies on a novel theoretical result to show that the restrictions of the LAX fragment ensure that for LAX programs, random tests over finite fields offer strong correctness guarantees. We show that an algorithm for polynomial identity testing (PIT) [34, 49] can be generalized to LAX programs, yielding a randomized algorithm for LAX program equivalence that can be made arbitrarily precise. Mirage uses this random algorithm to (probabilistically) ensure that each optimized program is equivalent to the input program.

**μGraph optimizer.** For each verified *μGraph*, Mirage’s *μGraph optimizer* maximizes its runtime performance by further considering potential tensor layouts, scheduling operators’ execution orders, and planning memory allocation at all of the kernel, thread block, and thread levels. Finally, Mirage returns an optimized tensor program based on the best discovered *μGraph* for each individual LAX subprogram.

**Evaluation results.** We evaluate Mirage on a variety of commonly used DNN benchmarks on NVIDIA A100 and H100 GPUs. Even for DNN benchmarks that are widely used and heavily optimized by existing systems such as the group-query attention used in LLMs [20], Mirage still outperforms

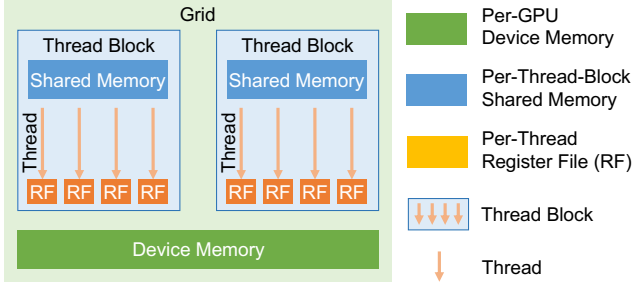


Figure 2: GPU compute and memory hierarchy.

current approaches by 1.1-2.9 $\times$ , by exploiting subtle custom kernels and optimizations missing in existing systems.

## 2 Multi-Level Graph Representation

Mirage uses a  $\mu$ Graph to specify the execution of a tensor program on GPUs. A  $\mu$ Graph contains hierarchical graphs at multiple levels to represent computation at the kernel, block, and thread levels<sup>2</sup>. This section first describes the GPU hierarchy and uses Figure 4 as a running example to introduce the key components of a  $\mu$ Graph.

**GPU hierarchy.** Figure 2 shows the hierarchy of today’s GPUs. Computations on GPUs are organized as *kernels*, each of which is a function executed simultaneously on multiple GPU cores in a single-program-multiple-data (SPMD) fashion. A kernel includes a grid of *thread blocks*, each of which is executed on one GPU streaming multiprocessor and includes multiple *threads* to perform computation on individual data elements. Each thread is associated with a per-thread *register file*, and all threads within a thread block can access *shared memory* to enable collective operations. Finally, all inputs and outputs of a kernel are stored in GPU *device memory*.

**Kernel graph.** Each tensor program corresponds to one *kernel graph*, where each node represents a kernel running on an entire GPU and each edge is a tensor shared between kernels. All tensors in a kernel graph are stored in GPU device memory since different kernels cannot share data in register file or shared memory. Each node in a kernel graph can be a *pre-defined* kernel operator supported by existing kernel libraries such as convolution by cuDNN [15] and matrix multiplication by cuBLAS [16]. In addition, to enable fine-grained inter-kernel optimizations such as kernel fusion, a node in a kernel graph can also be a *graph-defined* kernel operator, whose semantic and behavior are defined by a lower-level (i.e., block) graph. As an example, the kernel operator in Figure 4b is a graph-defined operator specified by a block graph.

<sup>2</sup>For simplicity, we use the term *block* to refer to a thread block of a CUDA kernel and *thread* to refer to a single CUDA thread.

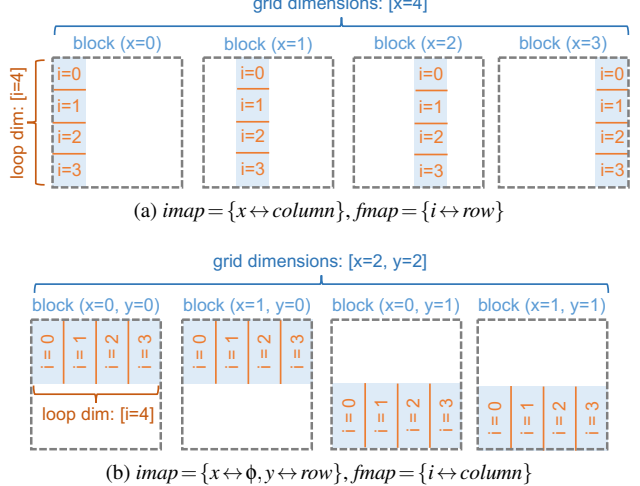


Figure 3: Demonstrating how an input tensor is partitioned across blocks and for-loop iterations with *imap* and *fmap*.

**Block graph.** A *block graph* specifies computation associated with a thread block<sup>3</sup>, where each node denotes a *block operator* which specifies computation within a block and each edge (blue arrows in Figure 4b) is a tensor shared between block operators. Mirage saves all intermediate tensors within a block graph in GPU *shared memory* for two considerations. First, GPU shared memory offers much higher bandwidth than device memory, and this design allows Mirage to reduce device memory access by maximally saving intermediate results in shared memory. Second, for tensors whose sizes exceed shared memory capacity and must be stored in device memory, Mirage uses these tensors to split computation into multiple block graphs, each of which only contains tensors in shared memory. This separation does not introduce additional access to device memory.

Each block graph is also associated with a few properties to specify its execution, which we introduce as follows.

**Grid dimensions.** All blocks within a kernel are organized by a mesh with up to 3 dimensions, identified as *x*, *y*, and *z*. A block graph is associated with up to three *grid dimensions* that specify the number of blocks along the *x*, *y*, and *z* dimensions. The block graph in Figure 4b launches 128 blocks.

First, for each input tensor to a graph-defined kernel operator (e.g., *X*, *G*, and *W* in the kernel graph in Figure 4b), the associated block graph contains an *imap*, which specifies how the input tensor is partitioned into sub-tensors for individual blocks. For each grid dimension (i.e., *x*, *y*, or *z*), the *imap* maps it to (1) a data dimension of the input tensor or (2) a special *replica dimension*  $\phi$ . For (1), the mapped data dimension is *equally partitioned* across blocks along the grid dimension. For (2), the input tensor is *replicated* across these blocks. As

<sup>3</sup>In the CUDA programming model, a kernel’s computation is defined as computations for independent thread blocks.

an example, the block graph in Figure 4b takes three inputs —  $\bar{X}$ ,  $\bar{G}$ , and  $\bar{W}$ , which represent the input tensors to each block. For  $\bar{W}$ , its  $imap = \{x \leftrightarrow d\}$  indicates that the  $d$  dimension of tensor  $W$  is partitioned into 128 equally sized chunks. As a result,  $\bar{W}$  is of shape  $[h=1024, d=32]$ .

Second, for each output tensor of a block graph (e.g.,  $\bar{Z}$  in Figure 4b), the block graph includes an *omap*, which specifies how the outputs of all blocks are concatenated to construct the final output of the kernel operator. In an *omap*, each grid dimension must map to a data dimension of the output tensor, since different blocks must save to disjoint tensors in device memory. For  $\bar{Z}$  of shape  $[b=16, d=32]$  in Figure 4b, its  $omap = \{x \leftrightarrow d\}$  indicates that blocks with the same  $x$  index are concatenated along the  $d$  dimension, resulting in a tensor  $Z$  of shape  $[b=16, d=4096]$ .

**For-loop dimensions.** To fit large input tensors in shared memory and allow cache reuse, a second property associated with each block graph is *for-loop dimensions*, which collectively specify how many times the block graph is executed to complete a kernel. For example, the block graph in Figure 4b has a for-loop dimension  $i=16$ , indicating it is executed 16 times to finish the associated graph-defined kernel operator. Correspondingly, each input tensor to a block graph is first sent to an *input iterator* that loads a part of the tensor (e.g.,  $\bar{X}$ ,  $\bar{G}$ , and  $\bar{W}$ ) from device memory to shared memory. Each input iterator is associated with an *fmap* to specify which part of the input tensor to load in each iteration. Formally, the *fmap* maps each for-loop dimension to (1) a data dimension of the input tensor or (2) the replica dimension  $\phi$ . Similar to the semantic of *imap*, the input tensor is equally partitioned along that dimension for (1) and replicated for (2). Figure 3 shows how an input matrix is partitioned across blocks and for-loop iterations with different *imap* and *fmap*.

In addition, a block graph contains *for-loop accumulators* (e.g., the two *Accum* operators in Figure 4b) to accumulate its output across iterations in shared memory. Similar to an input iterator, a for-loop accumulator is also associated with an *fmap* to specify how the output tensors of different iterations are combined to produce the accumulated results. Specifically, the *fmap* maps each for-loop dimension to either a data dimension, which results in concatenation of the output along that dimension, or the replica dimension  $\phi$ , which results in the output being accumulated in shared memory.

**Thread graph.** A *thread graph* further reduces the scope of computation from a block to a single thread. Similar to a block graph, each thread graph is also associated with *block dimensions*, which specify the organization of threads within the block, and *for-loop dimensions*, which define the total number of iterations to finish the defined computation. Each thread graph includes *input iterators*, each of which loads an input tensor (e.g.,  $\bar{A}$  and  $\bar{B}$  in Figure 4b) from GPU shared

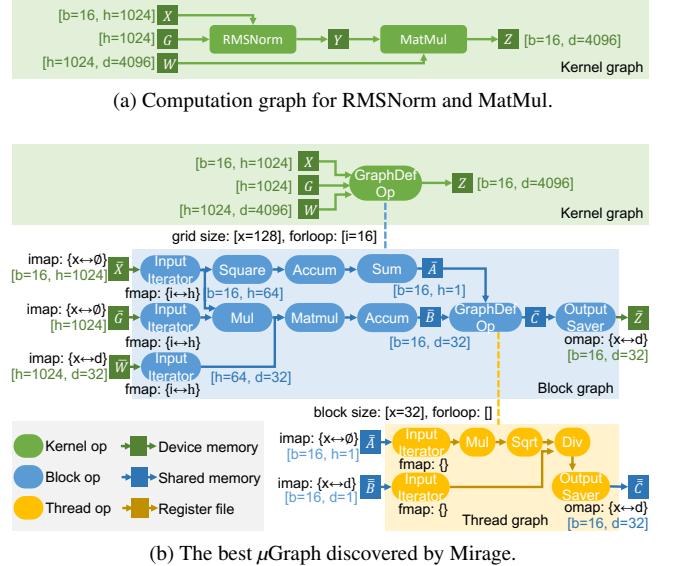


Figure 4: Figure 4a is the computation graph for RMSNorm and MatMul. Figure 4b shows the best  $\mu$ Graph discovered by Mirage for computing RMSNorm and MatMul, which fuses the computation in a single kernel to reduce device memory access and kernel launch overhead, outperforms existing approaches by  $1.9\times$ . Numbers in brackets indicate tensor shapes, and numbers in braces show the *imap*, *omap*, or *fmap* for the corresponding operators.

memory to register file, and *output savers*, each of which saves an output tensor from register file back to shared memory (e.g.,  $\bar{C}$ ). A thread graph is the lowest level graph in a  $\mu$ Graph and only contains pre-defined thread operators.

**Tensor layout.** Each tensor in the kernel, block, or thread graph is associated with a *tensor layout* (omitted in Figure 4 for simplicity), which specifies how the tensor is linearized in memory. Note that tensor layout only affects the execution performance of a  $\mu$ Graph and has no impact on its output.

**Comparison with prior work.** Prior work separately considers algebraic [24, 41] or schedule transformations [13, 28, 32], while  $\mu$ Graphs can represent both in a uniform way. Specifically, the grid and for-loop dimensions and their corresponding mappings (i.e., *imap*, *omap*, and *fmap*) to tensor dimensions constitute a comprehensive search space of possible schedules for graph-defined operators. The hierarchical graphs at the kernel, block, and thread levels allow Mirage to explore algebraic transformations at these levels.

### 3 Case Study: RMSNorm

In this section, we use the root mean square layer normalization (RMSNorm) [45] as a case study to demonstrate the

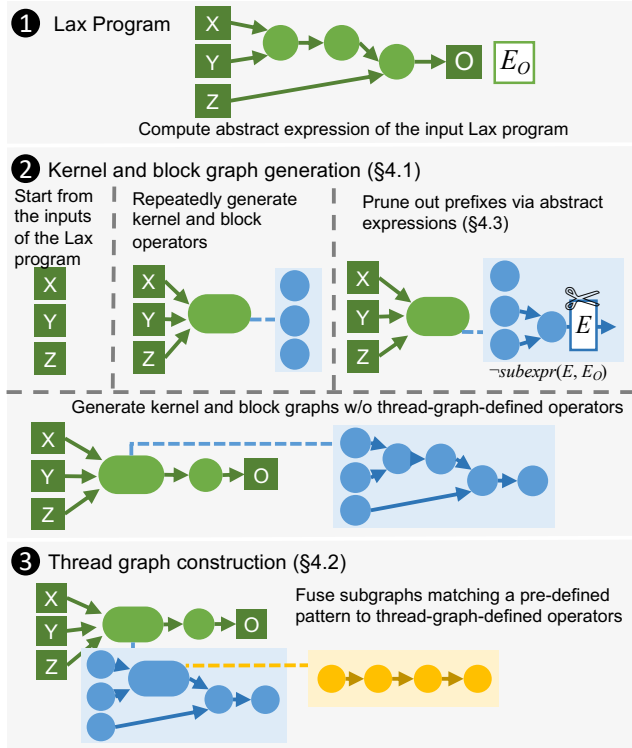


Figure 5: An overview of the  $\mu$ Graph generator.

advantages of the  $\mu$ Graph representation and Mirage’s super-optimization approach. RMSNorm is a widely used normalization technique by recent large language models such as LLAMA-2-70B [40]. Formally, RMSNorm takes two tensors  $X$  and  $G$  as inputs and regularizes the summed inputs of  $X$  according to the root mean square static:

$$Y_i = \frac{X_i G_i}{\text{RMS}(X)}, \text{RMS}(X) = \sqrt{\frac{1}{d} \sum_{j=1}^d X_j^2}, \quad (1)$$

where  $d$  is the hidden dimension size of  $X$ .

RMSNorm are generally followed by a matrix multiplication (MatMul). Figure 4a shows the computation graph of an RMSNorm and a MatMul operator, where  $X$  is the input tensor, and  $G$  and  $W$  denote two weight tensors. Existing ML compilers generally launch two separate kernels for RMSNorm and MatMul computations, since both of them internally perform reduction across an input dimension, making it challenging to fuse their computations in a single kernel. This approach requires storing intermediate results (i.e.,  $Y$ ) in device memory as different kernels cannot share data in shared memory or register files.

Figure 4b shows the best  $\mu$ Graph automatically discovered by Mirage for computing RMSNorm and MatMul in a single kernel. The computation is fused in a single graph-defined kernel operator to avoid saving intermediate results (i.e.,  $Y$ ) in device memory and reduce kernel launch overheads.

We highlight the key differences between the  $\mu$ Graph discovered by Mirage and the original  $\mu$ Graph. These differences involve discovering new custom kernels and combining algebraic and schedule transformations, making it infeasible to discover the final  $\mu$ Graph by separately considering algebraic and schedule transformations. First, Mirage reorders MatMul and the division of RMSNorm by leveraging the commutativity of matrix multiplication and element-wise division (algebraic transformation). Second, Mirage performs the accumulation in the root mean square (i.e.,  $\sum_j X_j^2$ ) and the accumulation in the matrix multiplication (i.e.,  $\sum_i X_i G_i W_{ik}$ ) in parallel (schedule transformation), avoiding writing the accumulation results to device memory. Next, Mirage instantiates a thread graph to perform a sequence of element-wise operators while maintaining all intermediate results in register files (schedule transformation). Finally, the best discovered  $\mu$ Graph uses a new custom kernel to fuse the computation of RMSNorm and MatMul, reducing device memory access and kernel launch overheads. This  $\mu$ Graph outperforms the hand-written kernels in existing systems by  $1.9\times$  and  $1.6\times$  on NVIDIA A100 and H100 GPUs.

## 4 Expression-Guided $\mu$ Graph Generator

---

### Algorithm 1

Mirage’s hybrid  $\mu$ Graph generation algorithm.

---

**Input:** A LAX program with a computation graph  $G_{\text{ref}}$   
**Output:** A set of  $\mu$ Graphs  $\mathcal{S}$

- 1:  $E_O \leftarrow \text{AbstractExpression}(G_{\text{ref}})$
- 2:  $\mathcal{S}_0, \mathcal{S} \leftarrow \emptyset, G \leftarrow \text{Inputs}(G_{\text{ref}})$
- 3: **GENERATEKERNELORBLOCKOPS**( $\mathcal{S}_0, G$ )
- 4: **CONSTRUCTTHREADGRAPHS**( $\mathcal{S}_0, \mathcal{S}$ )

5: **function** **GENERATEKERNELORBLOCKOPS**( $\mathcal{S}_0, G$ )  
6:    $\mathcal{S}_0 \leftarrow \mathcal{S}_0 \cup \{G\}$   
7:   **for all** kernel or block operator type  $type$ ; input set  $inputs$  **do**  
8:     **if**  $o := \text{CHECKANDCONSTRUCTOP}(G, inputs, type)$  is valid **then**  
9:       **GENERATENEXTKERNELOPERATOR**( $G \cup \{o\}$ )  
10: **function** **CHECKANDCONSTRUCTOP**( $G, inputs, type$ )  
11:   **if** **TensorShapeInference**( $inputs, type$ ) succeeds **then**  
12:     **if** **MemoryCheck**( $G, inputs, type$ ) **then**  
13:       **if** **IsSubexpression**(**AbstractExpression**( $G, inputs, type$ ),  $E_O$ ) **then**  
14:         **return** **ConstructOp**( $G, inputs, type$ )  
15:     **return** **Invalid**  
16: **function** **CONSTRUCTTHREADGRAPHS**( $\mathcal{S}_0, \mathcal{S}$ )  
17:    $\mathcal{P} \leftarrow$  pre-defined patterns  
18:   **for all**  $G \in \mathcal{S}_0$  **do**  
19:      $G_{\text{fused}} \leftarrow G$   
20:     **for all**  $(G_i, O_i) \in \mathcal{P}$  **do**  
21:       **for all** subgraph  $G'$  of  $G$  matching  $G_i$  **do**  
22:         Substitute  $G'$  with  $O_i$  in  $G_{\text{fused}}$   
23:      $\mathcal{S} \leftarrow \mathcal{S} \cup \{G_{\text{fused}}\}$

---

This section introduces the Mirage  $\mu$ Graph generator, which automatically discovers potential  $\mu$ Graphs for an input tensor program. To generate  $\mu$ Graphs that capture optimizations at all of the kernel, block, and thread levels, Mirage must explore a significantly larger search space than existing super-

optimizers that only consider optimizations at the kernel level. Mirage employs two key techniques to address this challenge. First, based on an important observation that optimizations at the kernel and block levels are substantially more critical to performance than optimizations at the thread level since accessing device and shared memory is orders of magnitude more expensive than accessing register file, Mirage’s  $\mu$ Graph generator employs a *hybrid approach*, considering all possible graphs up to a certain size at the kernel and block levels, and using a rule-based strategy to construct graphs at the thread level, which reduces the search space while retaining most performance optimizations. Second, to further prune the search space, Mirage introduces a pruning technique based on an abstraction of  $\mu$ Graphs called *abstract expression*, which reduces the number of  $\mu$ Graphs Mirage has to consider while providing a theoretical guarantee on the optimality of the discovered  $\mu$ Graphs.

## 4.1 Kernel and Block Graph Generation

Mirage generates kernel and block graphs incrementally and leverages several pruning techniques to reduce the search space, as shown in the second part of Figure 5. Specifically, Mirage maintains a *prefix* of a valid  $\mu$ Graph, iteratively extending it with new operators. Here, prefix  $G'$  of  $G$  is defined as a subgraph of  $G$  such that  $\forall u \in G', \forall (v, u) \in G, v \in G'$ . Mirage generates the next operator by enumerating the operator type *type* and the input tensor set *inputs* (line 7 in algorithm 1). If *type* represents a customized operator, Mirage will also enumerate its grid and for-loop dimensions.

Mirage checks tensor shape (line 11) and memory usage (line 12) before adding an operator, ensuring a valid prefix. A prefix passes the memory usage check if: (1) all tensors in the kernel graph can reside in device memory; and (2) all tensors in each block graph can fit in shared memory.

To ensure identical  $\mu$ Graphs are generated only once, Mirage defines the *canonical form* of  $\mu$ Graphs. Given a  $\mu$ Graph  $G$  with its operators in topological order  $o_1, \dots, o_n$ , the *index* of the  $j$ -th output of  $o_i$  is defined as a tuple  $(i, j)$ . Each operator  $o_i$  in  $G$  is assigned a *rank*  $(input_i, type_i)$ , where  $input_i$  is the list of input tensor indices of  $o_i$  and  $type_i$  is the operator type. A  $\mu$ Graph is in canonical form if the operators are in the increasing order of ranks. Mirage generates only  $\mu$ Graphs in canonical form by requiring that operators are added in the increasing order of ranks. This approach does not prune out any potential solutions, since each  $\mu$ Graph can be transformed to canonical form by reordering the operators.

In addition, Mirage utilizes the *abstract expression* technique to prune out prefixes that do not satisfy certain constraints, which will be introduced in §4.3.

Table 1: Operators supported by Mirage. The second column shows the levels of graphs supporting the operator (K, B and T stand for kernel, block and thread graphs, respectively). The last column defines the abstract expressions of the outputs of each operator.  $E$  is the mapping from tensors to the corresponding abstract expressions.

$\mu$ Graph Operator	Graph Level	Abstract Expression of Output Tensor
InIter	B	$E(\text{InIter}(X)) = E(X)$
OutSaver	B	$E(\text{OutSaver}(X)) = E(X)$
Matmul	K, B, T	$E(\text{Matmul}(X, Y)) = \text{sum}(k, \text{mul}(E(X), E(Y)))^1$
Sum	K, B, T	$E(\text{Sum}(d_r, k_r, X)) = \text{sum}(k_r, E(X))^2$
EwAdd	K, B, T	$E(\text{EwAdd}(X, Y)) = \text{add}(E(X), E(Y))$
EwMul	K, B, T	$E(\text{EwMul}(X, Y)) = \text{mul}(E(X), E(Y))$
EwDiv	K, B, T	$E(\text{EwDiv}(X, Y)) = \text{div}(E(X), E(Y))$
EwExp	K, B, T	$E(\text{EwExp}(X)) = \text{exp}(E(X))$
Repeat	K, B	$E(\text{Repeat}(X)) = E(X)$
Reshape	K, B	$E(\text{Reshape}(X)) = E(X)$
Sqr	K, B	$E(\text{Sqr}(X)) = \text{mul}(E(X), E(X))$
Sqrt	K, B	$E(\text{Sqrt}(X)) = \text{sqrt}(E(X))$
SiLU	K, B	$E(\text{SiLU}(X)) = \text{silu}(E(X))$
Accum	B	$E(\text{Accum}(X, m, i)) = \text{sum}(i, E(X)) \text{ if } m = \phi \text{ else } E(X)^3$

<sup>1</sup>  $k$  means the size of the last dimension of  $A$ , i.e., the reduction dimension. Matmul is performed on the inner most two dimensions and leading dimensions are batched.

<sup>2</sup> Sum along the dimension  $d_r$  for every  $k_r$  elements.

<sup>3</sup> Accumulate the results of  $i$  for-loop iterations along fmap  $m$ .

## 4.2 Thread Graph Construction

Mirage constructs thread graphs in a way similar to operator fusion, as shown in the third part of Figure 5 and line 5-line 9 in Algorithm 1. Specifically, Mirage has a set of pre-defined patterns  $\{(G_i, O_i)\}$  where each  $G_i$  is a graph consisting of block operators and  $O_i$  is a thread graph. Given a  $\mu$ Graph, Mirage traverses all its block graphs, replacing any subgraphs that match  $G_i$  with an operator defined by  $O_i$ .

## 4.3 Pruning via Abstract Expressions

When searching the space of possible  $\mu$ Graphs, we aim to avoid  $\mu$ Graph prefixes whose intermediate results cannot contribute to the desired computation. For example, for the input program  $X \cdot Z + Y \cdot Z$ , we can prune a prefix that computes  $X \cdot Y$ , but we should not prune one that computes  $X + Y$ , as  $(X + Y) \cdot Z$  is equivalent to the input program. However, how can we determine whether a prefix can contribute to a desired computation while searching for that computation? Below, we develop a pruning technique driven by this intuition that circumvents the “chicken and egg” problem via *abstraction*. First, we present the abstraction — *abstract expressions* — and then explain how it is used for pruning. Finally, we offer a theoretical guarantee that under certain conditions, this pruning does not exclude the optimal  $\mu$ Graph.

**Abstract expressions.** Recall that each edge in a  $\mu$ Graph corresponds to a tensor-valued function of the input tensors. Intuitively, abstract expressions abstract these functions by

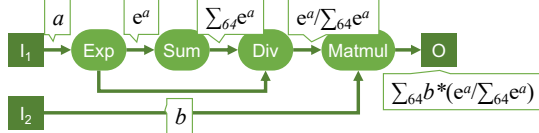


Figure 6: Illustration of abstract expressions. The abstract expressions of tensors are annotated on edges. A human-friendly notation is used here:  $e^a$  denotes  $\exp(a)$ ,  $\sum_k a$  denotes  $\text{sum}(k, a)$ ,  $a/b$  denotes  $\text{div}(a, b)$ , and  $a * b$  denotes  $\text{mul}(a, b)$ . The tensors  $I_1$ ,  $I_2$  and  $O$  are all  $64 \times 64$  matrices.

ignoring the differences between elements from the same input tensor. Formally, abstract expressions are first-order logic terms over the theory of integers and uninterpreted functions. In a  $\mu$ Graph, the abstract expression of each edge, denoted by  $E(\cdot)$ , is defined as shown in Table 1. During the computation of a  $\mu$ Graph’s abstract expression, all graph-defined operators are “inlined”. Specifically, the expressions computed for a graph-defined operator’s inputs serve as inputs to the lower-level graph, and the expressions for the outputs of this lower-level graph become the output expressions of the graph-defined operator. Figure 6 shows the abstract expressions for a subgraph of attention.

While abstract expressions capture some information about the function computed at each edge, they also abstract away much of it. For example, if  $X$  is a  $k \times k$  matrix, summing over the rows and summing over the columns lead to the same abstract expression— $\text{sum}(k, E(X))$ . But keeping  $k$  as part of the abstract expression is crucial for effective pruning.

**Abstract subexpression and pruning.** We use abstract expressions to prune the search space of  $\mu$ Graphs by formalizing two relations over abstract expressions: equivalence and abstract subexpression. We prune every  $\mu$ Graph prefix whose abstract expression is not a subexpression of some abstract expression equivalent to that of the input program. We formalize abstract expressions as uninterpreted functions in first-order logic over the theory of integer arithmetic and uninterpreted functions, and use an SMT solver to reason about them based on two sets of axioms in Table 2:  $A_{\text{eq}}$  and  $A_{\text{sub}}$ .  $A_{\text{eq}}$  axiomatizes equivalence between abstract expressions. As will become clear below, these axioms need not be sound—it is not necessary that  $\mu$ Graphs whose abstract expressions are equivalent are actually equivalent. (As mentioned earlier, non-equivalent  $\mu$ Graphs can have identical abstract expressions.)  $A_{\text{sub}}$  axiomatizes the subexpression relation between abstract expressions. The key property of this relation is that whenever a  $\mu$ Graph  $G_1$  is a prefix of  $G_2$ , meaning  $G_2$  can be obtained from  $G_1$  by adding more operators, then  $E(G_1)$  is an abstract subexpression of  $E(G_2)$ , i.e.,  $A_{\text{sub}} \models \text{subexpr}(E(G_1), E(G_2))$ , where  $\models$  denotes entailment modulo the theory of integer arithmetic and uninterpreted functions.

During the search, Algorithm 1 first computes the abstract

Table 2: Axiomatization of abstract expressions used for pruning. Mirage checks whether an abstract expression  $E_1$  is a subexpression of  $E_2$  by querying an SMT solver to check if  $\text{subexpr}(E_1, E_2)$  is entailed by these axioms. All variables are universally quantified.

Abstract Expression Property	
<i>Equivalence Axioms <math>A_{\text{eq}}</math></i>	<i>Subexpression Axioms <math>A_{\text{sub}}</math></i>
$\text{add}(x, y) = \text{add}(y, x)$	$\text{subexpr}(x, \text{add}(x, y))$
$\text{mul}(x, y) = \text{mul}(y, x)$	$\text{subexpr}(x, \text{mul}(x, y))$
$\text{add}(x, \text{add}(y, z)) = \text{add}(\text{add}(x, y), z)$	$\text{subexpr}(x, \text{div}(x, y))$
$\text{mul}(x, \text{mul}(y, z)) = \text{mul}(\text{mul}(x, y), z)$	$\text{subexpr}(y, \text{div}(x, y))$
$\text{add}(\text{mul}(x, z), \text{mul}(y, z)) = \text{mul}(\text{add}(x, y), z)$	$\text{subexpr}(x, \exp(x))$
$\text{add}(\text{div}(x, z), \text{div}(y, z)) = \text{div}(\text{add}(x, y), z)$	$\text{subexpr}(x, \text{sum}(i, x))$
$\text{mul}(x, \text{div}(y, z)) = \text{div}(\text{mul}(x, y), z)$	$\text{subexpr}(x, \text{sqrt}(i, x))$
$\text{div}(\text{div}(x, y), z) = \text{div}(x, \text{mul}(y, z))$	$\text{subexpr}(x, \text{sin}(i, x))$
$x = \text{sum}(1, x)$	$\text{subexpr}(x, x)$
$\text{sum}(i, \text{sum}(j, x)) = \text{sum}(i * j, x)$	$\text{subexpr}(x, y) \wedge \text{subexpr}(y, z) \rightarrow \text{subexpr}(x, z)$
$\text{sum}(i, \text{add}(x, y)) = \text{add}(\text{sum}(i, x), \text{sum}(i, y))$	
$\text{sum}(i, \text{mul}(x, y)) = \text{mul}(\text{sum}(i, x), y)$	
$\text{sum}(i, \text{div}(x, y)) = \text{div}(\text{sum}(i, x), y)$	

expression of the input LAX program,  $E_O$ , and prunes away any  $\mu$ Graph prefix  $G$  if  $A_{\text{eq}} \cup A_{\text{sub}} \not\models \text{subexpr}(E(G), E_O)$ . That is, we prune a graph if its abstract expression is not a subexpression of  $E_O$ . The check is performed by invoking an SMT solver (Z3 [18]). As an optimization, check results are cached and reused, since during the search Mirage may encounter multiple  $\mu$ Graphs with identical abstract expressions and SMT queries are relatively expensive.

**Theoretical guarantee and the pruning-optimality trade-off.** Intuitively, our pruning would keep any prefix that can lead to a  $\mu$ Graph whose abstract expression is equivalent (according to  $A_{\text{eq}}$ ) to that of the input LAX program. Formally:

**Theorem 1** (Pruning via Abstract Expressions). For an input  $\mu$ Graph  $G_0$ , and a  $\mu$ Graph  $G$  equivalent to  $G_0$ , if  $A_{\text{eq}} \models E(G_0) = E(G)$  then  $G$  will be generated by Algorithm 1.

*Proof.* By Tables 1 and 2, we show that for any operator  $op$ , if  $Y = op(X_1, \dots, X_n)$  then  $A_{\text{sub}} \models \text{subexpr}(E(X_i), E(Y))$  (for  $1 \leq i \leq n$ ). That is, an input to an operator is always an abstract subexpression of its output. By the reflexivity and transitivity axioms included in  $A_{\text{sub}}$ , it follows for any  $G'$  that is a prefix of  $G$ ,  $A_{\text{sub}} \models \text{subexpr}(E(G'), E(G))$ . Together with the assumption that  $A_{\text{eq}} \models E(G_0) = E(G)$ , it follows that  $A_{\text{eq}} \cup A_{\text{sub}} \models \text{subexpr}(E(G'), E(G_0))$ . Thus, any prefix of  $G$  will not be pruned, and  $G$  will be generated by Mirage.  $\square$

The theorem highlights the role of abstract expressions in solving the “chicken and egg” problem outlined above. To decide if a prefix  $\mu$ Graph is useful, we reason about whether it is a prefix of a useful computation *in the abstract*. The choice of the abstraction and of the axioms  $A_{\text{eq}}$  represents a tradeoff between optimality and pruning. As Theorem 1 shows, we are only guaranteed to find the optimal  $\mu$ Graph such that  $A_{\text{eq}}$  imply equivalence of its abstract expression to that of the input

program. The stronger the axioms, the theorem covers more  $\mu$ Graphs, but we also get less pruning because more prefixes would pass the subexpression test. In particular, note that  $A_{\text{eq}}$  does not consider cancellation (e.g.,  $\text{div}(\text{mul}(x, y), y) = y$ ). As a result, Mirage may miss some equivalent  $\mu$ Graphs. But including an axiom for cancellation of division and multiplication would make everything a subexpression of everything, therefore nulling the desired pruning. As our evaluation shows, our choice of  $A_{\text{eq}}$  yields a good balance between pruning and optimality.

## 5 Probabilistic Equivalence Verifier

Mirage’s *probabilistic equivalence verifier* checks if a candidate  $\mu$ Graph is equivalent to the desired LAX subprogram. The key idea is to evaluate both on *random inputs* in two finite fields. Using finite fields instead of floating point numbers not only avoids floating point errors, but also leads to a strong theoretical guarantee: the probability of accepting a non-equivalent  $\mu$ Graph can be made arbitrarily low.

For general programs, random tests can hardly provide any correctness guarantees. However, we show that for LAX programs (formally defined below), random testing provides a probabilistic correctness guarantee, and repeated tests can reduce the error probability to an arbitrarily small threshold.

Prior work [41] has applied a similar technique to check equivalence between tensor programs that only contain linear operators (e.g., matrix multiplication, convolution). We develop a random testing technique that also supports division and exponentiation, which are needed for many DNN optimizations (e.g., the RMSNorm example in §3).

Mirage verifies equivalence between LAX  $\mu$ Graphs (linear, division, and an exponential) defined below. We introduce the main theoretical results in §5.1 and present Mirage’s verification methodology in §5.2.

**Definition 5.1** (LAX  $\mu$ Graph). A  $\mu$ Graph  $G$  is a LAX  $\mu$ Graph if (1)  $G$  contains only multi-linear operators<sup>4</sup>, division, and exponentiation, and (2) every path from an input to an output in  $G$  includes at most one exponentiation.

### 5.1 Theoretical Foundations

Without loss of generality, we assume a LAX  $\mu$ Graph  $G$  takes  $n$  input tensors and produces one output tensor. Our theoretical results can directly generalize to LAX  $\mu$ Graph with multiple outputs. Since each LAX  $\mu$ Graph includes linear operators, divisions, and at most one exponentiation along each path, the computation for each entry of the output tensor can be

<sup>4</sup>Operator  $op$  with  $n$  inputs is multi-linear if  $op$  is linear to all inputs  $I_k$ :  
(1)  $\forall X, Y. op(I_1, \dots, I_{k-1}, X, I_{k+1}, \dots, I_n) + op(I_1, \dots, I_{k-1}, Y, I_{k+1}, \dots, I_n) = op(I_1, \dots, I_{k-1}, X + Y, I_{k+1}, \dots, I_n)$ , and  
(2)  $\alpha \cdot op(I_1, \dots, I_{k-1}, X, I_{k+1}, \dots, I_n) = op(I_1, \dots, I_{k-1}, \alpha \cdot X, I_{k+1}, \dots, I_n)$ .

Table 3: Arithmetic operations for random testing. Mirage selects two prime numbers  $p$  and  $q$  such that  $q$  divides  $p - 1$ .  $x_p$  and  $x_q$  are values from  $\mathbb{Z}_p$  and  $\mathbb{Z}_q$ , respectively.

Opt.	Opt. 1	Opt. 2	Output
Add.	$(x_p, x_q)$	$(y_p, y_q)$	$(x_p + y_p \pmod{p}, x_q + y_q \pmod{q})$
Sub.	$(x_p, x_q)$	$(y_p, y_q)$	$(x_p - y_p \pmod{p}, x_q - y_q \pmod{q})$
Mul.	$(x_p, x_q)$	$(y_p, y_q)$	$(x_p y_p \pmod{p}, x_q y_q \pmod{q})$
Div.	$(x_p, x_q)$	$(y_p, y_q)$	$(x_p y_p^{-1} \pmod{p}, x_q y_q^{-1} \pmod{q})$
Exp.	$(x_p, x_q)$	-	$(\omega^{x_q} \pmod{p}, -)$

expressed in the following form (by using standard identities such as  $\frac{a}{\frac{b}{d}} = \frac{ad}{bc}$ ,  $\frac{a}{b} + \frac{c}{d} = \frac{ad+bc}{bd}$ ,  $e^x e^y = e^{x+y}$ ):

$$\sum_{i=1}^k \frac{f_i}{g_i} e^{\left(\frac{h_i}{u_i}\right)}, \quad (2)$$

where  $f_i$ ,  $g_i$ ,  $h_i$ , and  $u_i$  ( $1 \leq i \leq k$ ) are polynomials over the entries of the input tensors.

The main theoretical result that underpins our randomized equivalence verification is the following theorem, which extends polynomial identity testing (PIT) [34, 49] on finite fields to LAX  $\mu$ Graphs. Note that the difference of two LAX  $\mu$ Graphs is also of the form of Equation (2). Therefore, identity testing of two LAX  $\mu$ Graphs can be done by testing if an expression of that form is zero. Because of the use of exponentiation, we use two finite fields instead of one.<sup>5</sup>

**Theorem 2.** Let  $\mathbb{Z}_p, \mathbb{Z}_q$  be the finite field of integers modulo  $p$  and  $q$ , respectively, where  $p, q$  are primes such that  $q$  divides  $p - 1$ . Let  $d, k \in \mathbb{N}$  s.t.  $dk^4 < q$ . Let  $f_1, \dots, f_k, g_1, \dots, g_k: \mathbb{Z}_p^N \rightarrow \mathbb{Z}_p$  be polynomials over  $\mathbb{Z}_p$  and  $h_1, \dots, h_k, u_1, \dots, u_k: \mathbb{Z}_q^M \rightarrow \mathbb{Z}_q$  be polynomials over  $\mathbb{Z}_q$ , where the degrees of all polynomials are at most  $d$ . Let  $\mathcal{G}$  be the set of  $q$ -th roots of unity in  $\mathbb{Z}_p$ . If  $h_i/u_i \not\equiv h_j/u_j$  for all  $i \neq j$ , and  $f_i, g_i, h_i \not\equiv 0$  for all  $i$ , then

$$\Pr_{\mathbf{x} \leftarrow \mathbb{Z}_p^N, \mathbf{y} \leftarrow \mathbb{Z}_q^M, \omega \leftarrow \mathcal{G}} \left[ \sum_{i=1}^k \frac{f_i(\mathbf{x})}{g_i(\mathbf{x})} \omega^{\frac{h_i(\mathbf{y})}{u_i(\mathbf{y})}} = 0 \wedge \mathcal{E} \right] \leq 1 - \frac{1}{k} + o\left(\frac{1}{k}\right),$$

where  $\mathcal{E}$  is the event that  $g_i(\mathbf{x}), u_i(\mathbf{y}) \neq 0$  for all  $i$ .

### 5.2 Random Tests over Finite Fields

Mirage leverages Theorem 2 to probabilistically verify the equivalence of two  $\mu$ Graphs by performing random testing over the finite fields  $\mathbb{Z}_p$  and  $\mathbb{Z}_q$  as defined in Theorem 2. To check the equivalence of two  $\mu$ Graphs, Mirage first generates the input tensors, where each entry is uniformly sampled from  $\mathbb{Z}_p \times \mathbb{Z}_q$ . Mirage also samples  $\omega$ , which is used for exponentiation, uniformly from all the  $q$ -roots of unity in  $\mathbb{Z}_p$ . Mirage

<sup>5</sup>We use two primes  $p$  and  $q$  for polynomial identity testing [34, 49] outside and inside the exponents, respectively. The condition  $q$  divides  $p - 1$  is to ensure the existence of  $q$ -th roots of unity in  $\mathbb{Z}_p$ .

then evaluates the two  $\mu$ Graphs over the finite fields for the same inputs using the operations defined in Table 3. As explained in §5.1,  $\mathbb{Z}_p$  and  $\mathbb{Z}_q$  are used outside and inside the exponent, respectively. All operations except exponentiation are implemented via modular arithmetic on  $\mathbb{Z}_p$  and  $\mathbb{Z}_q$  separately. Exponentiation uses the value  $x_q$  from  $\mathbb{Z}_q$  and transforms it to a value in  $\mathbb{Z}_p$  by computing  $\omega^{x_q} \pmod{p}$ . Note that in a LAX  $\mu$ Graph, exponentiation will be performed at most once along each path. Finally, Mirage checks whether the two  $\mu$ Graphs produce identical outputs. This process is repeated multiple times, and the two  $\mu$ Graphs pass the equivalence test if they pass all random tests. The following theorem, which follows from Theorem 2, shows that this process can yield an arbitrarily low error rate.

**Theorem 3.** Equivalent  $\mu$ Graphs always pass  $\mu$ Graph verification. For two non-equivalent  $\mu$ Graphs and a given probability threshold  $0 < \delta \leq 1$ , the  $\mu$ Graphs pass all  $\Omega(k \cdot \ln \frac{1}{\delta})$  random tests with probability at most  $\delta$ .

## 6 $\mu$ Graph Optimizer

For each verified  $\mu$ Graph, Mirage’s  *$\mu$ Graph optimizer* maximizes its performance by further performing *layout optimizations*, *operator scheduling*, and *memory planning*, as shown in Figure 1. Mirage defers these  $\mu$ Graph optimizations after verification for two reasons. First, these optimizations *do not* affect the correctness of the generated  $\mu$ Graphs; omitting them when generating  $\mu$ Graphs reduces the search space Mirage must consider, since  $\mu$ Graphs with the same graph topology but different choices of tensor layouts, operator orders, or memory allocation plans are considered identical by the  $\mu$ Graph generator. Second, considering these optimizations after verification also reduces the search space for these optimizations, since the  $\mu$ Graph optimizer only needs to optimize  $\mu$ Graphs that are functionally equivalent to the input.

**Tensor layouts.** The  $\mu$ Graph optimizer considers possible data layouts for all intermediate tensors at the kernel, block, and thread levels and chooses the best combinations to maximize performance. We formulate layout selection as a constrained optimization problem and use an integer linear programming (ILP) algorithm to solve it optimally. Specifically, for each tensor  $t$  and each possible layout  $l$  for  $t$ , we introduce a boolean variable  $B_{t,l}$  to indicate whether tensor  $t$  uses layout  $l$ . Operators at the kernel, block, and thread levels may impose various constraints on tensor layouts. For example, to use kernels in the cuBLAS library [16] to perform matrix multiplication, the innermost dimension of the two input tensors must be among the last two dimensions. These restrictions are converted into a series of linear constraints on  $B_{t,l}$ . Different tensor layouts may lead to varying performance. For example, some input tensor layouts support bulk copies from device to shared memory, while others do not. Mirage introduces

Table 4: DNN benchmarks used in our evaluation.

Name	Description	Base Architecture
GQA	Group-query attention	LLaMA-3-70B [20]
QKNorm	QK normalization with attention	Chameleon-7B [37]
RMSNorm	RMS normalization with linear	LLaMA-2-7B [40]
LoRA	Low-rank adaptation	GPT-3-7B-LoRA [6]
GatedMLP	Gated multi-layer perceptron	Falcon-7B [10]
nTrans	Normalized Transformer	nGPT-1B [25]

a cost function to model the performance of each operator under different layout choices. Mirage uses an off-the-shelf ILP solver (i.e., Z3 [18]) to find an optimal layout strategy that satisfies all layout constraints while minimizing cost.

**Operator scheduling.** In a  $\mu$ Graph, there are multiple topological orders to execute operators, and different orders may yield different performance. For a given input  $\mu$ Graph, the  $\mu$ Graph optimizer identifies an efficient strategy to schedule operators by minimizing thread-level synchronization within each thread block (i.e., `__syncthreads()` in CUDA). To achieve this goal, Mirage labels each node with a *depth*, defined as the length of the longest path from any input operator to that node. Mirage uses a dynamic programming algorithm to compute the depth of each node and schedules all operators in ascending order of their depths. This approach minimizes the number of thread-level synchronizations required in the generated CUDA kernel, as Mirage only needs to insert synchronization points between operators of different depths.

**Memory planning.** A third class of post-verification optimizations is memory planning, which determines the memory offsets for all intermediate tensors at the kernel, block, and thread levels. Mirage formulates memory planning as a *dynamic storage allocation* task and exhaustively enumerates all allocation plans to discover an optimal strategy.

## 7 Implementation

Mirage is implemented in 30K lines of code in C++, CUDA, and Python. Kernel operators are implemented with the cuDNN and cuBLAS libraries [15, 16], and block and thread operators are implemented using cutLASS [2] and CUDA functions. For each input tensor program, Mirage automatically generates and verifies potential  $\mu$ Graphs. For each verified  $\mu$ Graph, Mirage produces CUDA source code for all custom kernels of the  $\mu$ Graph and compiles the code into binary using the CUDA compiler. This approach enables just-in-time (JIT) compilation and deployment for general tensor programs, and the generated kernels can be directly integrated into a PyTorch program with a few lines of code changes. The SMT and ILP solvers of Mirage are implemented using Z3 4.12.6 [18].

Our implementation supports the operators listed in Table 1. Mirage can be extended to include new operators, such as variants of convolution or matrix multiplication, at the kernel, block, and/or thread levels. To support a new linear operator, Mirage requires (1) a float-pointing implementation of the operator at the kernel, block, and/or thread levels, which is used by the  $\mu$ Graph optimizer to generate CUDA kernels, (2) an implementation of the operator over modular arithmetic (see §5), and (3) an extension to the abstract expression axioms  $A_{\text{eq}}$  and  $A_{\text{sub}}$  for it (see §4.3).

To utilize Theorems 2 and 3, random tests should be performed with sufficiently large prime numbers  $p$  and  $q$  and should be iterated multiple times. Our current implementation uses the largest values of  $p$  and  $q$  whose product fits in 16-bit integers (i.e.,  $p=227, q=113$ ) to perform the random testing on GPUs, leveraging Mirage’s GPU optimizations such as maintaining intermediate results in GPU shared memory, which allows Mirage to accelerate its search procedure. We also use a single random test without iterating it and compare all elements of the output tensors. We note that this equivalence verification procedure does not introduce false negatives. While false positives may be introduced, we have not observed any in practice. For these reasons, we consider this procedure to be sufficient for the search process and plan to add an additional verification step that provides the theoretical guarantees only for the best  $\mu$ Graph at the end of the optimization process.

**Equivalence verification for non-LAX programs.** While Mirage can generate  $\mu$ Graphs for arbitrary input tensor programs, the probabilistic equivalence verifier is restricted to LAX programs and does not support certain DNN operators such as ReLU [29]. As an alternative, we have developed a solver-based verifier for arbitrary tensor programs. The verifier relies on user-provided mathematical properties of individual operators (e.g., linearity, associativity, commutativity, and distributivity) defined in first-order logic and uses these properties to verify equivalence using an automated theorem prover. Compared to the probabilistic equivalence verifier, the solver-based verifier supports more general programs, while requiring additional manual effort to specify the properties for each new operator. A detailed discussion of the solver-based verifier is beyond the scope of this paper.

## 8 Evaluation

### 8.1 Experimental Setup

Since Mirage is a superoptimizer for LAX programs, we focus our evaluation on various DNN benchmarks commonly used by existing DNNs, each of which is a LAX program. These benchmarks provide the most fine-grained way to compare the performance of Mirage and existing systems. Table 4 shows the six benchmarks in our evaluation. GQA, RMSNorm, and

GatedMLP are the main building blocks of large language models (LLMs). QKNorm introduces query-key normalization before attention to enhance model convergence [37]. LoRA enables low-rank adaptation for fine-tuning a DNN on different tasks. In addition, we also evaluate how Mirage-generated kernels can improve the end-to-end performance of DNNs, including Chameleon [37], nGPT [25], LLaMA-3 [20], and LoRA [23].

The experiments were performed on a NVIDIA 40GB A100 and a NVIDIA 40GB H100 GPU. All our benchmarks fit on a single GPU except GQA (used for LLaMA-2-70B), which is generally parallelized across four GPUs using tensor model parallelism [36]. Therefore, we evaluate GQA under the tensor model parallelism strategy (i.e., the 8 key-value heads are equally partitioned across four GPUs). Since the performance of Mirage and all baselines depends only on the shapes of the input tensors, we repeat each experiment 1,000 times using random inputs and report the average run time.

One of our benchmarks, LoRA, requires concatenation to express a common tensor optimization: fusing two matrix multiplications via concatenation. To support this optimization in Mirage, we add a new linear operator that takes four inputs and computes  $f(W, X, Y, Z) = (W \| X) \times (Y \| Z)$ , where  $\|$  is tensor concatenation. This operator is equivalent to computing  $W \times Y + X \times Z$ . We define the abstract expression associated with the new operator as:  $E(f(W, X, Y, Z)) = \text{add}(\text{sum}(k_1, \text{mul}(E(W), E(Y))), \text{sum}(k_2, \text{mul}(E(X), E(Z))))$ , where  $k_1$  and  $k_2$  are the last dimensions of  $W$  and  $X$ .

Unless otherwise stated, Mirage considers up to 5 operators in the kernel graph and up to 11 operators in each block graph.

## 8.2 Benchmark Results

Figure 7 compares the performance of Mirage with existing tensor program optimizers on six DNN benchmarks on NVIDIA A100 and H100 GPUs. All systems use half-precision floating points to serve these DNN benchmarks. TASO [24] and PET [41] are DNN superoptimizers that automatically generate graph optimizations at the kernel level. PyTorch [31] uses the highly engineered cuDNN and cuBLAS libraries [15, 16] to perform DNN operators on GPUs. TensorRT and its LLM variant TensorRT-LLM include a set of manually designed and highly optimized kernels for common tensor operators such as attention [38]. FlashAttention and its inference variant FlashDecoding are manually designed and implemented kernels for fast attention computation [17, 22]. Finally, Triton [39] is a schedule-based optimizer to generate high-performance kernels and has been deployed in existing systems, achieving better performance than other schedule-based optimizers.

Compared to the best existing approaches, Mirage improves the performance of these benchmarks by 1.1-2.9 $\times$  by combining algebraic transformations, schedule transformations, and the generation of new custom kernels. §3 shows the best

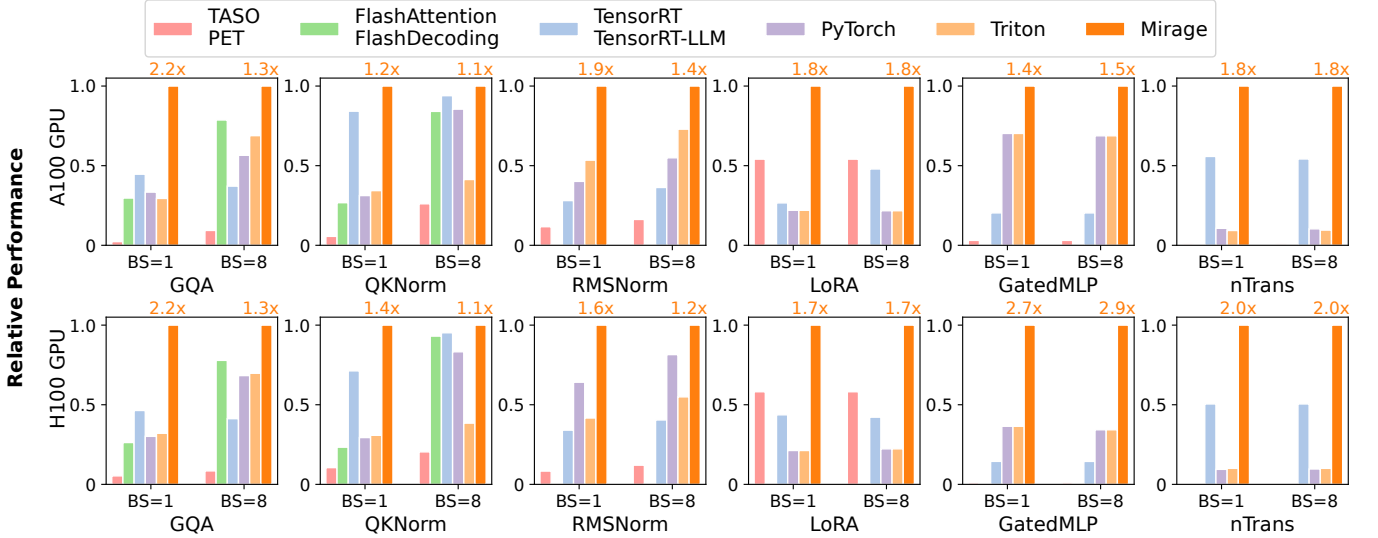
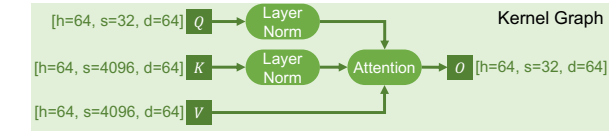
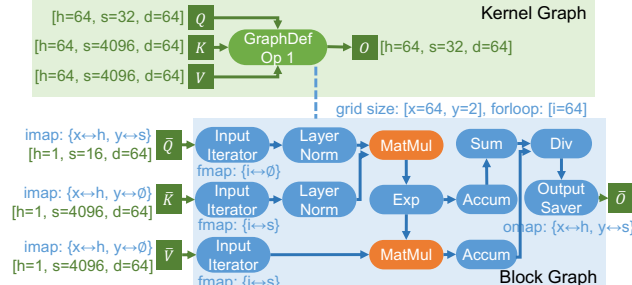


Figure 7: Comparing Mirage with existing systems for 6 benchmarks on an A100 and an H100 GPU. The performance of all systems are normalized by Mirage (higher is better). Numbers above the Mirage bars show the speedup over the best baselines.



(a) The kernel graph for QKNorm and attention in existing systems.



(b) The best  $\mu$ Graph discovered by Mirage for QKNorm and attention.

Figure 8: Comparing the  $\mu$ Graphs used by existing optimizers and Mirage for QKNorm and attention.

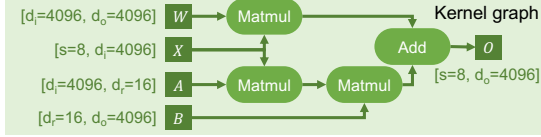
discovered  $\mu$ Graphs for RMSNorm. Next, we present a case study for the other benchmarks.

**GQA.** Group-query attention is the backbone of LLMs and has been heavily optimized by existing frameworks. For example, FlashAttention and FlashDecoding are expert-designed attention kernels and have been adopted in existing LLM inference systems [17]. Mirage discovers existing expert-designed kernels as well as other  $\mu$ Graphs that outperform them by up to  $2.2\times$ . The speedup is achieved by two additional optimizations on top of existing hand-written kernels. First, current approaches rely on heuristics to determine the grid dimen-

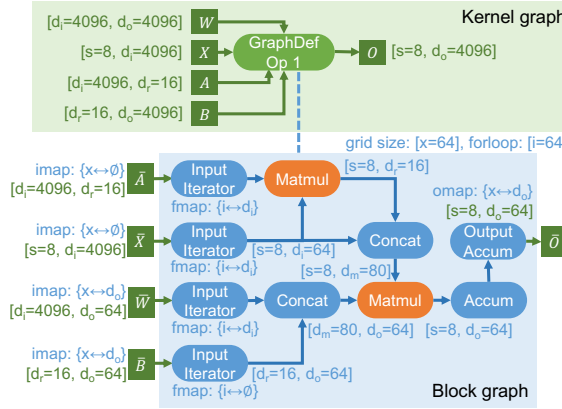
sions for GQA, which are suboptimal in certain scenarios. For example, TensorRT-LLM launches the attention kernel with grid dimensions of  $(8, 2, 1)$  and  $(8, 2, 8)$  for GQA when the batch sizes are 1 and 8, respectively. Both configurations cannot fully utilize all A100 and H100 GPUs, which have 108 and 132 SMs respectively. On the other hand, Mirage automatically searches for the best grid dimensions for each  $\mu$ Graph, resulting in fully utilized SMs.

Second, existing approaches use fixed tensor dimensions to parallelize GQA across thread blocks. For example, FlashAttention [17] parallelizes attention across blocks using the *sample*, *head*, and *query sequence* dimensions, while FlashDecoding and TensorRT-LLM leverage the *sample*, *head*, and *key-value sequence* dimensions. Both strategies are efficient for conventional multi-head attention with many attention heads but suboptimal for GQA with limited attention heads. In contrast, Mirage automatically selects the most efficient dimensions among sample, KV heads, query sequence, and key-value sequence, and uses different  $\mu$ Graphs for different attention scenarios, reducing device memory access by up to  $7\times$  compared to the heuristics used in existing systems. Implementing Mirage’s  $\mu$ Graphs in existing systems is possible but requires extensive engineering effort to support different kernels for different scenarios, while Mirage automatically generates them and verify their correctness.

**QKNorm.** To reduce model divergence, several recent DNNs introduce query-key normalization (QKNorm) into the Transformer architecture [37]. QKNorm applies layer normalization to the query and key vectors before attention, as shown in Figure 8a. These additional normalization layers are not yet supported by existing attention implementations (e.g.,



(a) The kernel graph for LoRA in existing systems.



(b) The best  $\mu$ Graph discovered by Mirage for LoRA.

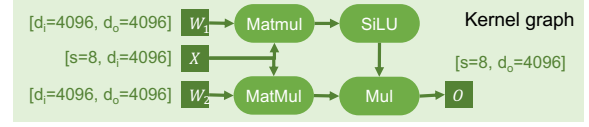
Figure 9: Comparing the tensor programs used by existing optimizers and by Mirage for LoRA:  $O = W \times X + B \times A \times X$ . Note that both matrices  $A$  and  $B$  are low-rank.

FlashAttention and TensorRT-LLM) and require launching separate kernels for normalization and attention.

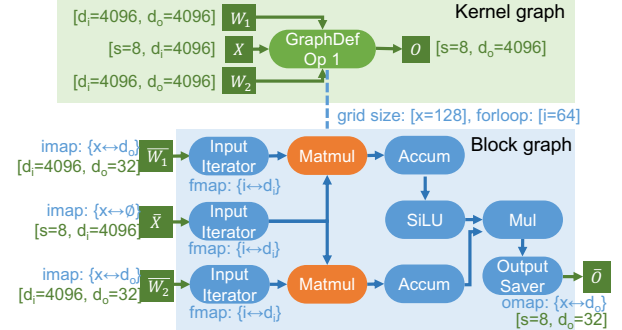
Mirage automatically discovers a  $\mu$ Graph that integrates QKNorm and attention computation into a custom kernel, as shown in Figure 8b. The  $\mu$ Graph reorganizes the attention computation to enable fusion with the two layer normalizations, which avoids writing intermediate results to GPU device memory and reduces the kernel execution time by 1.1-1.4 $\times$ .

**LoRA.** Low-rank adaptation (LoRA) introduces a pair of low-rank adapters to the linear operators of a pre-trained DNN to improve its predictive performance for downstream tasks. Existing tensor program optimizers launch separate kernels for the original linear operator and the two new linear operators in LoRA (Figure 9a), which introduces high kernel launch overheads since the LoRA operators involve very low computational costs. Figure 9b shows the best  $\mu$ Graph discovered by Mirage for LoRA, which fuses the three Matmuls and the subsequent Add into a single kernel. Mirage reorganizes the computation into two thread-block level Matmuls by leveraging the following algebraic transformation:  $W \times X + B \times A \times X = (W \parallel B) \times (X \parallel (A \times X))$ . The Concats in Figure 9b do not involve any computation and are performed by updating tensor offsets in GPU shared memory. This  $\mu$ Graph reduces the execution cost of LoRA by 1.7-1.8 $\times$ .

**GatedMLP.** Gated multi-layer perceptron is commonly used in DNNs to capture non-linear representations. We use the GatedMLP configuration introduced in Falcon-7B [10],



(a) The kernel graph for GatedMLP.



(b) The best  $\mu$ Graph discovered by Mirage for GatedMLP.

Figure 10: Comparing the  $\mu$ Graphs used by existing optimizers and Mirage for GatedMLP.

whose kernel graph is shown in Figure 10a. Existing tensor program optimizers generally fuse the two Matmuls in a single kernel to reduce GPU device memory access since the input tensor  $X$  only needs to be loaded once. However, this approach still requires launching multiple kernels and storing intermediate results (i.e., the output of the two Matmuls) in device memory as the SiLU activation and elementwise multiplication are not fused with the Matmuls.

In contrast, the best  $\mu$ Graph discovered by Mirage (Figure 10b) performs the two Matmuls in parallel in the same block graph and fuses the remaining computation (i.e., SiLU and Mul) as a post-processing step into the block graph. This approach yields 1.4-1.5 $\times$  speedups on A100 GPUs and 2.7-2.9 $\times$  speedups on H100 GPUs.

**nTrans.** To accelerate model training, nGPT introduces normalized Transformer, which normalizes all intermediate results in Transformer. Formally, the computation is defined as  $y = \text{Norm}(x + \alpha(\text{Norm}(h - x)))$ , where  $\text{Norm}$  is a normalization layer, and  $x$ ,  $h$ , and  $\alpha$  are the input tensors. Existing systems launch three separate kernels for nTrans since it interleaves normalization and elementwise addition and multiplication. Mirage automatically discovers a  $\mu$ Graph that fuses the computation into a single kernel and stores all intermediate results in the GPU shared memory, reducing the kernel execution time by 1.8-2.0 $\times$  compared to the best existing systems.

### 8.3 End-to-end Results

In addition to the microbenchmark performance, we also evaluate how Mirage-generated kernels reduce the end-to-end latency of commonly used DNNs. Mirage supports just-in-time compilation and deployment, and its generated kernels

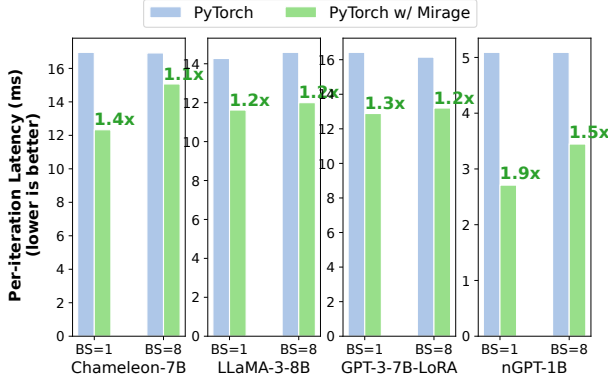


Figure 11: Comparing the end-to-end inference performance of PyTorch and PyTorch with Mirage-generated kernels.

Table 5: Ablation study on Mirage’s techniques to accelerate  $\mu$ Graph generation. We evaluate the impact of multi-threading and abstract expressions on search time for RMSNorm.

Max # Ops in a Block Graph	Mirage	Mirage w/o Multithreading	Mirage w/ Abstract Expression
5	11 sec	58 sec	768 sec
6	16 sec	93 sec	19934 sec
7	22 sec	150 sec	> 10 h
8	24 sec	152 sec	> 10 h
9	26 sec	166 sec	> 10 h
10	26 sec	166 sec	> 10 h
11	28 sec	183 sec	> 10 h

can be directly integrated in PyTorch programs. We compare PyTorch with its native handwritten CUDA kernels and PyTorch with Mirage-generated kernels on four DNN models. Figure 11 shows the results. Mirage reduces the end-to-end latency of these models by 1.1–1.9 $\times$  by automatically generating highly optimized kernels. Note that the improvement is achieved by a few lines of code changes to the PyTorch programs.

#### 8.4 Optimization Time and Ablation Study

Generally, Mirage takes up to 4 hours to optimize a LAX program. Note that this optimization is a one-time cost before deployment on the target hardware. This section provides more detailed results and an ablation study for Mirage’s search procedure. We evaluate how our techniques allow Mirage to explore large  $\mu$ Graphs while maintaining low search time. We focus on two techniques: pruning via abstract expressions (§4.3) and multi-threading. Table 5 reports the search times for RMSNorm as we adjust the maximum number of operators in a block graph. Multi-threading significantly reduces the search time, while pruning via abstract expressions is crucial for the scalability of Mirage. Specifically, the pruning techniques allow Mirage to explore  $\mu$ Graphs whose block graph can each have at most 11 operators, while disabling

abstract expressions restricts Mirage to consider up to 6 operators in a block graph in order to finish the search in 10 hours. Note that Mirage needs to consider 11 operators in a block graph in order to discover the  $\mu$ Graph shown in Figure 4 for RMSNorm.

## 9 Related Work

**Manually-designed kernels.** Many existing frameworks, such as TensorFlow XLA [1, 9], PyTorch [31], and TensorRT [38], rely on GPU experts to manually design and implement kernels for ML operators. Recently, significant engineering effort has been dedicated to manually designing, implementing, and optimizing GPU kernels for commonly used DNNs (known as foundation models [12]). For example, to optimize attention computation [42], recent work has introduced various kernels based on FlashAttention [4, 5, 17, 22]. Due to the increasing complexity of modern GPU architectures (e.g., tensor cores in A100s [26] and thread block clusters in H100s [7]), manually designed kernels may miss subtle optimizations that are hard to discover manually.

**Superoptimization-based approaches.** Superoptimization was originally introduced to find optimal code for instruction sequences [11, 27, 33]. Recent work has applied superoptimization techniques to tensor programs [24, 41, 44, 47]. All these attempts only consider algebraic transformations at the kernel level and cannot discover sophisticated optimizations that require jointly considering algebraic and schedule transformations at all of the kernel, block, and thread levels. Our evaluation shows that Mirage largely outperforms existing DNN superoptimizers, demonstrating the significance of multi-level joint optimizations.

**Schedule-based approaches.** Recent work has introduced ML compilers that automatically optimize the schedule of kernel executions on GPUs. For example, TVM [13, 14], An-sor [46], and Triton [39], among others [19, 21, 48] are based on the idea of algorithm-schedule separation introduced in Halide and search for an optimized schedule to execute a given algorithm on GPUs. Schedule-based approaches rely on users to explicitly specify the algorithm for each kernel and their performance is limited to the provided algorithms.

**Multi-level graph representations.** Welder [35] and AS-PEN [30] introduce multi-level tile graphs that bear some similarity to Mirage’s  $\mu$ Graphs, as both representations follow the GPU memory hierarchy. However, prior work focuses on scheduling transformations, while Mirage covers these optimizations and also considers algebraic transformations and discovery of new custom kernels. Most optimizations shown in the paper are outside the scope of prior work.

## 10 Conclusion

This paper proposes Mirage, the first multi-level superoptimizer for tensor programs. Mirage introduces a hierarchy graph representation to specify a tensor program at the kernel, thread block, and thread levels of the GPU compute hierarchy, and uses a novel pruning technique based on abstraction to significantly reduce the search space Mirage needs to consider while providing a certain optimality guarantee. Mirage outperforms existing tensor program optimizers by 1.1-2.9× even for widely used and heavily optimized DNNs.

## Acknowledgment

We thank Tianqi Chen, Phillip Gibbons, Bohan Hou, Muyan Hu, and other CMU Catalyst members for their feedback on this work. This research is partially supported by NSF awards CNS-2147909, CNS-2211882, and CNS-2239351, and research awards from Amazon, Cisco, Google, Meta, Oracle, Qualcomm, and Samsung.

## References

- [1] Xla: Optimizing compiler for tensorflow. <https://www.tensorflow.org/xla>, 2017. 13
- [2] Nvidia/cutlass: Cuda templates for linear algebra subroutines. <https://github.com/NVIDIA/cutlass>, 2019. 9
- [3] Tensorflow graph optimization with grappler. [https://www.tensorflow.org/guide/graph\\_optimization](https://www.tensorflow.org/guide/graph_optimization), 2019. 1
- [4] Transformer related optimizations. <https://github.com/NVIDIA/FasterTransformer>, 2020. 13
- [5] Flash-decoding for long-context inference. <https://crfm.stanford.edu/2023/10/12/flashdecoding.html>, 2023. 2, 13
- [6] Llama-7b-lora. <https://huggingface.co/Laurie/llama7b-lora-merged/tree/main>, 2023. 9
- [7] Nvidia h100 tensor core gpu. <https://www.nvidia.com/en-us/data-center/h100/>, 2023. 13
- [8] A Triton implementation of the FlashAttention2 algorithm. <https://triton-lang.org/main/getting-started/tutorials/06-fused-attention.html>, 2023. 2
- [9] Martín Abadi, Paul Barham, Jianmin Chen, Zhifeng Chen, Andy Davis, Jeffrey Dean, Matthieu Devin, Sanjay Ghemawat, Geoffrey Irving, Michael Isard, Manjunath Kudlur, Josh Levenberg, Rajat Monga, Sherry Moore, Derek G. Murray, Benoit Steiner, Paul Tucker, Vijay Vasudevan, Pete Warden, Martin Wicke, Yuan Yu, and Xiaoqiang Zheng. Tensorflow: A system for large-scale machine learning. In *Proceedings of the 12th USENIX Conference on Operating Systems Design and Implementation*, OSDI, 2016. 1, 13
- [10] Ebtesam Almazrouei, Hamza Alobeidli, Abdulaziz Alshamsi, Alessandro Cappelli, Ruxandra Cojocaru, Merouane Debbah, Etienne Goffinet, Daniel Heslow, Julien Launay, Quentin Malartic, Badreddine Noune, Baptiste Pannier, and Guilherme Penedo. Falcon-40B: an open large language model with state-of-the-art performance. 2023. 9, 12
- [11] Sorav Bansal and Alex Aiken. Automatic generation of peephole superoptimizers. In *Proceedings of the 12th International Conference on Architectural Support for Programming Languages and Operating Systems*, ASPLOS XII, 2006. 13
- [12] Rishi Bommasani, Drew A. Hudson, Ehsan Adeli, Russ Altman, Simran Arora, Sydney von Arx, Michael S. Bernstein, Jeannette Bohg, Antoine Bosselut, Emma Brunskill, Erik Brynjolfsson, Shyamal Buch, Dallas Card, Rodrigo Castellon, Niladri Chatterji, Annie Chen, Kathleen Creel, Jared Quincy Davis, Dora Demszky, Chris Donahue, Moussa Doumbouya, Esin Durmus, Stefano Ermon, John Etchemendy, Kawin Ethayarajh, Li Fei-Fei, Chelsea Finn, Trevor Gale, Lauren Gillespie, Karan Goel, Noah Goodman, Shelby Grossman, Neel Guha, Tatsunori Hashimoto, Peter Henderson, John Hewitt, Daniel E. Ho, Jenny Hong, Kyle Hsu, Jing Huang, Thomas Icard, Saahil Jain, Dan Jurafsky, Pratyusha Kalluri, Siddharth Karamcheti, Geoff Keeling, Fereshte Khani, Omar Khattab, Pang Wei Koh, Mark Krass, Ranjay Krishna, Rohith Kuditipudi, Ananya Kumar, Faisal Ladhak, Mina Lee, Tony Lee, Jure Leskovec, Isabelle Levent, Xiang Lisa Li, Xuechen Li, Tengyu Ma, Ali Malik, Christopher D. Manning, Suvir Mirchandani, Eric Mitchell, Zanele Munyikwa, Suraj Nair, Avanika Narayan, Deepak Narayanan, Ben Newman, Allen Nie, Juan Carlos Niebles, Hamed Nilforoshan, Julian Nyarko, Giray Ogut, Laurel Orr, Isabel Papadimitriou, Joon Sung Park, Chris Piech, Eva Portelance, Christopher Potts, Aditi Raghunathan, Rob Reich, Hongyu Ren, Frieda Rong, Yusuf Roohani, Camilo Ruiz, Jack Ryan, Christopher Ré, Dorsa Sadigh, Shiori Sagawa, Keshav Santhanam, Andy Shih, Krishnan Srinivasan, Alex Tamkin, Rohan Taori, Armin W. Thomas, Florian Tramèr, Rose E. Wang, William Wang, Bohan Wu, Jiajun Wu, Yuhuai Wu, Sang Michael Xie, Michihiro Yasunaga, Jiaxuan You, Matei Zaharia, Michael Zhang, Tianyi Zhang, Xikun Zhang, Yuhui Zhang, Lucia Zheng, Kaitlyn Zhou, and Percy Liang. On the opportunities and risks of foundation models, 2022. 13

[13] Tianqi Chen, Thierry Moreau, Ziheng Jiang, Haichen Shen, Eddie Q. Yan, Leyuan Wang, Yuwei Hu, Luis Ceze, Carlos Guestrin, and Arvind Krishnamurthy. TVM: end-to-end optimization stack for deep learning. *CoRR*, abs/1802.04799, 2018. [1](#), [4](#), [13](#)

[14] Tianqi Chen, Lianmin Zheng, Eddie Yan, Ziheng Jiang, Thierry Moreau, Luis Ceze, Carlos Guestrin, and Arvind Krishnamurthy. Learning to optimize tensor programs. In *Advances in Neural Information Processing Systems 31*, NeurIPS’18. 2018. [13](#)

[15] Sharan Chetlur, Cliff Woolley, Philippe Vandermersch, Jonathan Cohen, John Tran, Bryan Catanzaro, and Evan Shelhamer. cudnn: Efficient primitives for deep learning. *CoRR*, abs/1410.0759, 2014. [3](#), [9](#), [10](#)

[16] Dense Linear Algebra on GPUs. <https://developer.nvidia.com/cUBLAS>, 2016. [3](#), [9](#), [10](#)

[17] Tri Dao, Daniel Haziza, Francisco Massa, and Grigory Sizov. Flash-decoding for long-context inference, 2023. [2](#), [10](#), [11](#), [13](#)

[18] Leonardo De Moura and Nikolaj Bjørner. Z3: An efficient smt solver. In *Proceedings of the Theory and Practice of Software, 14th International Conference on Tools and Algorithms for the Construction and Analysis of Systems*, TACAS’08/ETAPS’08, 2008. [7](#), [9](#)

[19] Siyuan Feng, Bohan Hou, Hongyi Jin, Wuwei Lin, Junru Shao, Ruihang Lai, Zihao Ye, Lianmin Zheng, Cody Hao Yu, Yong Yu, and Tianqi Chen. Tensorir: An abstraction for automatic tensorized program optimization, 2022. [13](#)

[20] Aaron Grattafiori, Abhimanyu Dubey, Abhinav Jauhri, Abhinav Pandey, Abhishek Kadian, Ahmad Al-Dahle, Aiesha Letman, Akhil Mathur, Alan Schelten, Alex Vaughan, Amy Yang, Angela Fan, Anirudh Goyal, Anthony Hartshorn, Aobo Yang, Archi Mitra, Archie Sravankumar, Artem Korenev, Arthur Hinsvark, Arun Rao, Aston Zhang, Aurelien Rodriguez, Austen Gregerson, Ava Spataru, Baptiste Roziere, Bethany Biron, Binh Tang, Bobbie Chern, Charlotte Caucheteux, Chaya Nayak, Chloe Bi, Chris Marra, Chris McConnell, Christian Keller, Christophe Touret, Chunyang Wu, Corinne Wong, Cristian Canton Ferrer, Cyrus Nikolaidis, Damien Allonsius, Daniel Song, Danielle Pintz, Danny Livshits, Danny Wyatt, David Esiobu, Dhruv Choudhary, Dhruv Mahajan, Diego Garcia-Olano, Diego Perino, Dieuwke Hupkes, Egor Lakomkin, Ehab AlBadawy, Elina Lobanova, Emily Dinan, Eric Michael Smith, Filip Radenovic, Francisco Guzmán, Frank Zhang, Gabriel Synnaeve, Gabrielle Lee, Georgia Lewis Anderson, Govind Thattai, Graeme Nail, Gregoire Mialon, Guan Pang, Guillem Cucurell, Hailey Nguyen, Hannah Korevaar, Hu Xu, Hugo Touvron, Iliyan Zarov, Imanol Arrieta Ibarra, Isabel Kloumann, Ishan Misra, Ivan Evtimov, Jack Zhang, Jade Copet, Jaewon Lee, Jan Geffert, Jana Vranes, Jason Park, Jay Mahadeokar, Jeet Shah, Jelmer van der Linde, Jennifer Billock, Jenny Hong, Jenya Lee, Jeremy Fu, Jianfeng Chi, Jianyu Huang, Jiawen Liu, Jie Wang, Jiecao Yu, Joanna Bitton, Joe Spisak, Jongsoo Park, Joseph Rocca, Joshua Johnstun, Joshua Saxe, Jun-teng Jia, Kalyan Vasudevan Alwala, Karthik Prasad, Kartikeya Upasani, Kate Plawiak, Ke Li, Kenneth Heafield, Kevin Stone, Khalid El-Arini, Krithika Iyer, Kshitiz Malik, Kuenley Chiu, Kunal Bhalla, Kushal Lakhota, Lauren Rantala-Yearly, Laurens van der Maaten, Lawrence Chen, Liang Tan, Liz Jenkins, Louis Martin, Lovish Madaan, Lubo Malo, Lukas Blecher, Lukas Landzaat, Luke de Oliveira, Madeline Muzzi, Mahesh Pasupuleti, Mannat Singh, Manohar Paluri, Marcin Kardas, Maria Tsimpoukelli, Mathew Oldham, Mathieu Rita, Maya Pavlova, Melanie Kambadur, Mike Lewis, Min Si, Mitesh Kumar Singh, Mona Hassan, Naman Goyal, Narjes Torabi, Nikolay Bashlykov, Nikolay Bogoychev, Niladri Chatterji, Ning Zhang, Olivier Duchenne, Onur Çelebi, Patrick Alrassy, Pengchuan Zhang, Pengwei Li, Petar Vasic, Peter Weng, Prajjwal Bhargava, Pratik Dubal, Praveen Krishnan, Punit Singh Koura, Puxin Xu, Qing He, Qingxiao Dong, Ragavan Srinivasan, Raj Ganapathy, Ramon Calderer, Ricardo Silveira Cabral, Robert Stojnic, Roberta Raileanu, Rohan Maheswari, Rohit Girdhar, Rohit Patel, Romain Sauvestre, Ronnie Polidoro, Roshan Sumbaly, Ross Taylor, Ruan Silva, Rui Hou, Rui Wang, Saghar Hosseini, Sahana Chennabasappa, Sanjay Singh, Sean Bell, Seohyun Sonia Kim, Sergey Edunov, Shaoliang Nie, Sharan Narang, Sharath Raparthy, Sheng Shen, Shengye Wan, Shruti Bhosale, Shun Zhang, Simon Vandenhende, Soumya Batra, Spencer Whitman, Sten Sootla, Stephane Collot, Suchin Gururangan, Sydney Borodinsky, Tamar Herman, Tara Fowler, Tarek Sheasha, Thomas Georgiou, Thomas Scialom, Tobias Speckbacher, Todor Mihaylov, Tong Xiao, Ujjwal Karn, Vedanuj Goswami, Vibhor Gupta, Vignesh Ramanathan, Viktor Kerkez, Vincent Gonguet, Virginie Do, Vish Vogeti, Vitor Albiero, Vladan Petrovic, Weiwei Chu, Wenhan Xiong, Wenyin Fu, Whitney Meers, Xavier Martinet, Xiaodong Wang, Xiaofang Wang, Xiaoqing Ellen Tan, Xide Xia, Xinfeng Xie, Xuchao Jia, Xuewei Wang, Yaelle Goldschlag, Yashesh Gaur, Yasmine Babaei, Yi Wen, Yiwen Song, Yuchen Zhang, Yue Li, Yuning Mao, Zacharie Delpierre Coudert, Zheng Yan, Zhengxing Chen, Zoe Papakipos, Aaditya Singh, Aayushi Srivastava, Abha Jain, Adam Kelsey, Adam Shajnfeld, Adithya Gangidi, Adolfo Victoria, Ahuva Goldstand, Ajay Menon, Ajay Sharma, Alex Boesenberg, Alexei Baevski, Allie Feinstein, Amanda Kallet, Amit Sangani, Amos Teo, Anam Yunus, Andrei Lupu,

Andres Alvarado, Andrew Caples, Andrew Gu, Andrew Ho, Andrew Poulton, Andrew Ryan, Ankit Ramchandani, Annie Dong, Annie Franco, Anuj Goyal, Aparajita Saraf, Arkabandhu Chowdhury, Ashley Gabriel, Ashwin Bharambe, Assaf Eisenman, Azadeh Yazdan, Beau James, Ben Maurer, Benjamin Leonhardi, Bernie Huang, Beth Loyd, Beto De Paola, Bhargavi Paranjape, Bing Liu, Bo Wu, Boyu Ni, Braden Hancock, Bram Wasti, Brandon Spence, Brani Stojkovic, Brian Gamido, Britt Montalvo, Carl Parker, Carly Burton, Catalina Mejia, Ce Liu, Changhan Wang, Changkyu Kim, Chao Zhou, Chester Hu, Ching-Hsiang Chu, Chris Cai, Chris Tindal, Christoph Feichtenhofer, Cynthia Gao, Damon Civin, Dana Beaty, Daniel Kreymer, Daniel Li, David Adkins, David Xu, Davide Testuggine, Delia David, Devi Parikh, Diana Liskovich, Didem Foss, Dingkang Wang, Duc Le, Dustin Holland, Edward Dowling, Eissa Jamil, Elaine Montgomery, Eleonora Presani, Emily Hahn, Emily Wood, Eric-Tuan Le, Erik Brinkman, Esteban Arcuate, Evan Dunbar, Evan Smothers, Fei Sun, Felix Kreuk, Feng Tian, Filippos Kokkinos, Firat Ozgenel, Francesco Caggioni, Frank Kanayet, Frank Seide, Gabriela Medina Florez, Gabriella Schwarz, Gada Badeer, Georgia Swee, Gil Halpern, Grant Herman, Grigory Sizov, Guangyi, Zhang, Guna Lakshminarayanan, Hakan Inan, Hamid Shojanazeri, Han Zou, Hannah Wang, Hanwen Zha, Haroun Habeeb, Harrison Rudolph, Helen Suk, Henry Aspegren, Hunter Goldman, Hongyuan Zhan, Ibrahim Damlaj, Igor Molybog, Igor Tufanov, Ilias Leontiadis, Irina-Elena Veliche, Itai Gat, Jake Weissman, James Geboski, James Kohli, Janice Lam, Japhet Asher, Jean-Baptiste Gaya, Jeff Marcus, Jeff Tang, Jennifer Chan, Jenny Zhen, Jeremy Reizenstein, Jeremy Teboul, Jessica Zhong, Jian Jin, Jingyi Yang, Joe Cummings, Jon Carvill, Jon Shepard, Jonathan McPhie, Jonathan Torres, Josh Ginsburg, Junjie Wang, Kai Wu, Kam Hou U, Karan Saxena, Kartikay Khandelwal, Katayoun Zand, Kathy Matosich, Kaushik Veeraraghavan, Kelly Michelena, Keqian Li, Kiran Jagadeesh, Kun Huang, Kunal Chawla, Kyle Huang, Lailin Chen, Lakshya Garg, Lavender A, Leandro Silva, Lee Bell, Lei Zhang, Liangpeng Guo, Licheng Yu, Liron Moshkovich, Luca Wehrstedt, Madiam Khabsa, Manav Avalani, Manish Bhatt, Martynas Mankus, Matan Hasson, Matthew Lennie, Matthias Reso, Maxim Groshev, Maxim Naumov, Maya Lathi, Meghan Keneally, Miao Liu, Michael L. Seltzer, Michal Valko, Michelle Restrepo, Mihir Patel, Mik Vyatskov, Mikayel Samvelyan, Mike Clark, Mike Macey, Mike Wang, Miquel Jubert Hermoso, Mo Metanat, Mohammad Rastegari, Munish Bansal, Nandhini Santhanam, Natascha Parks, Natasha White, Navyata Bawa, Nayan Singhal, Nick Egebo, Nicolas Usunier, Nikhil Mehta, Nikolay Pavlovich Laptev, Ning Dong, Norman Cheng, Oleg Chernoguz, Olivia Hart, Omkar Salpekar, Ozlem

Kalinli, Parkin Kent, Parth Parekh, Paul Saab, Pavan Balaji, Pedro Rittner, Philip Bontrager, Pierre Roux, Piotr Dollar, Polina Zvyagina, Prashant Ratanchandani, Pritish Yuvraj, Qian Liang, Rachad Alao, Rachel Rodriguez, Rafi Ayub, Raghotham Murthy, Raghu Nayani, Rahul Mitra, Rangaprabhu Parthasarathy, Raymond Li, Rebekkah Hogan, Robin Battey, Rocky Wang, Russ Howes, Ruty Rinott, Sachin Mehta, Sachin Siby, Sai Jayesh Bondu, Samyak Datta, Sara Chugh, Sara Hunt, Sargun Dhillon, Sasha Sidorov, Satadru Pan, Saurabh Mahajan, Saurabh Verma, Seiji Yamamoto, Sharadh Ramaswamy, Shaun Lindsay, Shaun Lindsay, Sheng Feng, Shenghao Lin, Shengxin Cindy Zha, Shishir Patil, Shiva Shankar, Shuqiang Zhang, Shuqiang Zhang, Sinong Wang, Sneha Agarwal, Soji Sajuyigbe, Soumith Chintala, Stephanie Max, Stephen Chen, Steve Kehoe, Steve Satterfield, Sudarshan Govindaprasad, Sumit Gupta, Summer Deng, Sungmin Cho, Sunny Virk, Suraj Subramanian, Sy Choudhury, Sydney Goldman, Tal Remez, Tamar Glaser, Tamara Best, Thilo Koehler, Thomas Robinson, Tianhe Li, Tianjun Zhang, Tim Matthews, Timothy Chou, Tzook Shaked, Varun Vontimitta, Victoria Ajayi, Victoria Montanez, Vijai Mohan, Vinay Satish Kumar, Vishal Mangla, Vlad Ionescu, Vlad Poenaru, Vlad Tiberiu Mihailescu, Vladimir Ivanov, Wei Li, Wenchen Wang, Wenwen Jiang, Wes Bouaziz, Will Constable, Xiaocheng Tang, Xiaojian Wu, Xiaolan Wang, Xilun Wu, Xinbo Gao, Yaniv Kleinman, Yanjun Chen, Ye Hu, Ye Jia, Ye Qi, Yenda Li, Yilin Zhang, Ying Zhang, Yossi Adi, Youngjin Nam, Yu, Wang, Yu Zhao, Yuchen Hao, Yundi Qian, Yunlu Li, Yuzi He, Zach Rait, Zachary DeVito, Zef Rosnbrick, Zhaoduo Wen, Zhenyu Yang, Zhiwei Zhao, and Zhiyu Ma. The llama 3 herd of models, 2024. 2, 9, 10

- [21] Bastian Hagedorn, Bin Fan, Hanfeng Chen, Cris Cecka, Michael Garland, and Vinod Grover. Graphene: An ir for optimized tensor computations on gpus. In *Proceedings of the 28th ACM International Conference on Architectural Support for Programming Languages and Operating Systems, Volume 3*, ASPLOS 2023, page 302–313, New York, NY, USA, 2023. Association for Computing Machinery. 13
- [22] Ke Hong, Guohao Dai, Jiaming Xu, Qiuli Mao, Xiuhong Li, Jun Liu, Kangdi Chen, Yuhang Dong, and Yu Wang. Flashdecoding++: Faster large language model inference on gpus, 2024. 10, 13
- [23] Edward J Hu, Yelong Shen, Phillip Wallis, Zeyuan Allen-Zhu, Yuanzhi Li, Shean Wang, Lu Wang, and Weizhu Chen. Lora: Low-rank adaptation of large language models. *arXiv preprint arXiv:2106.09685*, 2021. 10
- [24] Zhihao Jia, Oded Padon, James Thomas, Todd Warszawski, Matei Zaharia, and Alex Aiken. Taso: Optimizing

deep learning computation with automatic generation of graph substitutions. In *Proceedings of the 27th ACM Symposium on Operating Systems Principles, SOSP ’19*, page 47–62, New York, NY, USA, 2019. Association for Computing Machinery. 1, 2, 4, 10, 13

[25] Ilya Loshchilov, Cheng-Ping Hsieh, Simeng Sun, and Boris Ginsburg. nGPT: Normalized transformer with representation learning on the hypersphere, 2024. 9, 10

[26] Stefano Markidis, Steven Wei Der Chien, Erwin Laure, Ivy Bo Peng, and Jeffrey S. Vetter. Nvidia tensor core programmability, performance & precision. In *2018 IEEE International Parallel and Distributed Processing Symposium Workshops (IPDPSW)*. IEEE, May 2018. 13

[27] Henry Massalin. Superoptimizer: a look at the smallest program. In *ACM SIGARCH Computer Architecture News*, volume 15, 1987. 13

[28] Ravi Teja Mullapudi, Andrew Adams, Dillon Sharlet, Jonathan Ragan-Kelley, and Kayvon Fatahalian. Automatically scheduling halide image processing pipelines. *ACM Trans. Graph.*, 35(4), 2016. 4

[29] Vinod Nair and Geoffrey E. Hinton. Rectified linear units improve restricted boltzmann machines. In *Proceedings of the 27th International Conference on International Conference on Machine Learning, ICML’10*, pages 807–814, USA, 2010. Omnipress. 10

[30] Jongseok Park, Kyungmin Bin, Gibum Park, Sangtae Ha, and Kyunghan Lee. Aspen: Breaking operator barriers for efficient parallelization of deep neural networks. In A. Oh, T. Naumann, A. Globerson, K. Saenko, M. Hardt, and S. Levine, editors, *Advances in Neural Information Processing Systems*, volume 36, pages 68625–68638. Curran Associates, Inc., 2023. 13

[31] Tensors and Dynamic neural networks in Python with strong GPU acceleration. <https://pytorch.org>, 2017. 1, 10, 13

[32] Jonathan Ragan-Kelley, Connelly Barnes, Andrew Adams, Sylvain Paris, Frédo Durand, and Saman Amarasinghe. Halide: A language and compiler for optimizing parallelism, locality, and recomputation in image processing pipelines. In *Proceedings of the 34th ACM SIGPLAN Conference on Programming Language Design and Implementation, PLDI ’13*, 2013. 1, 4

[33] Eric Schkufza, Rahul Sharma, and Alex Aiken. Stochastic superoptimization. In *ACM SIGPLAN Notices*, volume 48, 2013. 13

[34] J. T. Schwartz. Fast probabilistic algorithms for verification of polynomial identities. *J. ACM*, 27(4):701–717, oct 1980. 2, 8

[35] Yining Shi, Zhi Yang, Jilong Xue, Lingxiao Ma, Yuqing Xia, Ziming Miao, Yuxiao Guo, Fan Yang, and Lidong Zhou. Welder: Scheduling deep learning memory access via tile-graph. In *17th USENIX Symposium on Operating Systems Design and Implementation (OSDI 23)*, pages 701–718, Boston, MA, July 2023. USENIX Association. 13

[36] Mohammad Shoeybi, Mostofa Patwary, Raul Puri, Patrick LeGresley, Jared Casper, and Bryan Catanzaro. Megatron-lm: Training multi-billion parameter language models using model parallelism. *CoRR*, abs/1909.08053, 2019. 10

[37] Chameleon Team. Chameleon: Mixed-modal early-fusion foundation models, 2024. 9, 10, 11

[38] NVIDIA TensorRT: Programmable inference accelerator. <https://developer.nvidia.com/tensorrt>, 2017. 10, 13

[39] Philippe Tillet, H. T. Kung, and David Cox. Triton: an intermediate language and compiler for tiled neural network computations. In *Proceedings of the 3rd ACM SIGPLAN International Workshop on Machine Learning and Programming Languages, MAPL 2019*, page 10–19, New York, NY, USA, 2019. Association for Computing Machinery. 2, 10, 13

[40] Hugo Touvron, Louis Martin, Kevin Stone, Peter Albert, Amjad Almahairi, Yasmine Babaei, Nikolay Bashlykov, Soumya Batra, Prajwala Bhargava, Shruti Bhosale, et al. Llama 2: Open foundation and fine-tuned chat models, 2023. 5, 9

[41] Haojie Wang, Jidong Zhai, Mingyu Gao, Zixuan Ma, Shizhi Tang, Liyan Zheng, Yuanzhi Li, Kaiyuan Rong, Yuanyong Chen, and Zhihao Jia. PET: Optimizing tensor programs with partially equivalent transformations and automated corrections. In *15th USENIX Symposium on Operating Systems Design and Implementation (OSDI 21)*, pages 37–54. USENIX Association, July 2021. 1, 2, 4, 8, 10, 13

[42] Thomas Wolf, Lysandre Debut, Victor Sanh, Julien Chaumond, Clement Delangue, Anthony Moi, Pierrette Cistac, Tim Rault, Rémi Louf, Morgan Funtowicz, Joe Davison, Sam Shleifer, Patrick von Platen, Clara Ma, Yacine Jernite, Julien Plu, Canwen Xu, Teven Le Scao, Sylvain Gugger, Mariama Drame, Quentin Lhoest, and Alexander M. Rush. Transformers: State-of-the-art machine learning for pytorch, tensorflow, and jax. <https://github.com/huggingface/transformers>, 2022. 2, 13

[43] Yichen Yang, Phitchaya Mangpo Phothilimtha, Yisu Remy Wang, Max Willsey, Sudip Roy, and Jacques Pienaar. Equality saturation for tensor graph superoptimization, 2021. 1

[44] Yichen Yang, Phitchaya Phothilimhana, Yisu Wang, Max Willsey, Sudip Roy, and Jacques Pienaar. Equality Saturation for Tensor Graph Superoptimization. *Proceedings of Machine Learning and Systems*, 3:255–268, March 2021. 13

[45] Biao Zhang and Rico Sennrich. Root mean square layer normalization, 2019. 4

[46] Lianmin Zheng, Chengfan Jia, Minmin Sun, Zhao Wu, Cody Hao Yu, Ameer Haj-Ali, Yida Wang, Jun Yang, Danyang Zhuo, Koushik Sen, Joseph E. Gonzalez, and Ion Stoica. Ansor : Generating high-performance tensor programs for deep learning. *CoRR*, abs/2006.06762, 2020. 1, 13

[47] Liyan Zheng, Haojie Wang, Jidong Zhai, Muyan Hu, Zixuan Ma, Tuowei Wang, Shuhong Huang, Xupeng Miao, Shizhi Tang, Kezhao Huang, and Zhihao Jia. EINNET: Optimizing tensor programs with Derivation-Based transformations. In *17th USENIX Symposium on Operating Systems Design and Implementation (OSDI 23)*, pages 739–755, Boston, MA, July 2023. USENIX Association. 13

[48] Size Zheng, Yun Liang, Shuo Wang, Renze Chen, and Kaiwen Sheng. Flextensor: An automatic schedule exploration and optimization framework for tensor computation on heterogeneous system. In *Proceedings of the Twenty-Fifth International Conference on Architectural Support for Programming Languages and Operating Systems, ASPLOS ’20*, page 859–873, New York, NY, USA, 2020. Association for Computing Machinery. 13

[49] Richard Zippel. Probabilistic algorithms for sparse polynomials. In *International symposium on symbolic and algebraic manipulation*, pages 216–226. Springer, 1979. 2, 8